Journal of Hydrology 663 (2025) 134310

Contents lists available at ScienceDirect

Journal of Hydrology

journal homepage: www.elsevier.com/locate/jhydrol

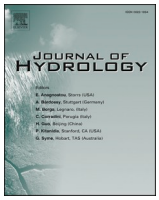

Research papers

Relative importance of uncertain model parameters driving water fluxes in a land surface model

Aronne Dell'Oca [a], David Luttenauer [b], Alberto Guadagnini [a], Sylvain Weill [b], Philippe Ackerer [a,b,*]

[a] Dipartimento di Ingegneria Civile e Ambientale, Politecnico di Milano, Milano, Italy
[b] Institut Terre et Environnement de Strasbourg, Université de Strasbourg, CNRS, ENGEES, F-67000 Strasbourg, France

ARTICLE INFO

This manuscript was handled by A. Bardossy, Editor-in-Chief, with the assistance of Basant Yadav, Associate Editor

Keywords:
Catchment hydrology
Water cycle
Groundwater recharge

ABSTRACT

We analyze the way temporal distributions of key components of the water cycle are influenced by typically uncertain parameters embedded in a Land Surface Model (LSM). The main objective of this study is to gain a clearer quantitative understanding of how uncertainty in model parameters affects land surface model outputs is critical for improving water balance assessment and supporting resource management. We explore the sensitivity of transpiration, evaporation, and groundwater recharge dynamics to uncertain parameters in the modular NIHM (Normally Integrated Hydrological Model) LSM. The latter is employed to simulate realistic field conditions (in terms of, e.g., climate, vegetation, and soil type) across a one-year period associated with two contrasting watersheds in the Vosges region (France), differing in vegetation and soil characteristics. A key novelty of our work lies in the simultaneous application of multiple global sensitivity analysis metrics (including moment-based and moment-independent indices) to enable a richer and multi-faceted evaluation of how input uncertainty propagates to various statistical aspects (mean, variance, or full distribution) of model outputs. This multi-metric approach reveals temporal dynamics of parameter sensitivity, also depending on the model output (statistical) moment considered. Our results suggest that evaporation is primarily controlled by energy transfer through the canopy and drainage properties of the top litter layer. Transpiration drivers differ across sites, vegetation traits, albedo, and canopy radiation attenuation playing central roles. Groundwater recharge appears to be sensitive to only a limited subset of parameters, such as root zone drainage and rainfall interception. These types of insights are valuable in the context of future model calibration phases, as they enable one to prioritize parameters requiring detailed field characterization and to support simplification of model structures without hampering accuracy.

1. Introduction

Since the work of Manabe (1969), Land Surface Models (LSMs) have become critical tools for modeling energy balance, water cycle, vegetation dynamics, and their feedbacks. They constitute one of the key routines employed in (*a*) General Circulation Models (GCMs) to evaluate the effects of climate change on the Earth surface as well as in (*b*) modeling workflows routinely used for water resources management. Over the past decades, numerous LSMs have been developed and adapted to a wide range of environmental settings, each reflecting different conceptualizations and parameterizations (e.g. Blyth et al., 2021; Fisher and Koven, 2020; Overgaard et al., 2006; and references therein). These models are characterized by various levels of complexity and include, e.g., LSMs described in Decharme et al. (2011), Niu et al. (2011), Maneta and Silverman (2013), Lawrence et al. (2019), Wiltshire et al. (2019), or Yokohata et al. (2019). This diversity highlights the current gaps in our understanding of land surface processes related to energy and water dynamics.

A primary purpose of a LSM is to simulate exchanges of energy and water between the land surface, the underground, and the atmosphere. Due to the variety of processes that are mathematically rendered therein, LSMs embed numerous input parameters related to vegetation, energy transfer and water fluxes across the atmosphere and in the soil. Many of these parameters (e.g., soil attributes or vegetation characteristics) are difficult to quantify through direct measurements and may vary across scales and locations. These elements typically lead to

* Corresponding author at: Institut Terre et Environnement de Strasbourg, Université de Strasbourg, CNRS, ENGEES, F-67000 Strasbourg, France.
E-mail address: ackerer@unistra.fr (P. Ackerer).

https://doi.org/10.1016/j.jhydrol.2025.134310
Received 4 April 2025; Received in revised form 9 August 2025; Accepted 21 September 2025
Available online 26 September 2025

uncertainty in our knowledge of the values of such parameters (Beven and Smith, 2014). In case a target model output is not (or only minimally) affected by the particular values associated with certain parameters, it may be appropriate to rely on typical literature values for these. It is then important to properly identify parameters that significantly impact model outputs and understand their role in driving model behaviour.

In this context, sensitivity analysis enables one to quantitatively rank the influence that diverse uncertain model parameters involved in the mathematical rendering of different processes might exert onto model results/outputs of interest. Thus, sensitivity analysis should be considered as an integral and essential step in diagnosis, characterization, and understanding of complex models of hydrological systems (Ferretti et al., 2016; Song et al., 2015; Vemuri et al., 1969; Razavi et al., 2021). Sensitivity analyses can yield valuable information about LSMs development, potentially simplifying mathematical representations, and streamline LSMs calibration by omitting uninfluential parameters (McCuen, 1973).

Sensitivity analysis has been previously performed for LSMs in a variety of contexts and settings, with reference to diverse LSM output(s). Demarty et al. (2005) perform a sensitivity analysis of soil heat conduction flux, sensible heat flux, latent heat flux, water content of the upper five soil centimetres and local directional brightness temperature considering 35 input parameters associated with the physically-based model SiSPAT-RS (Braud et al., 1995). Their findings indicate the saturated water content of the upper 5 cm of soil and the thermal infrared brightness temperature as the most influent model parameters. Liang and Guo (2003) compare the sensitivity of evapotranspiration, total runoff, sensible heat flux and soil moisture to 5 model parameters that appear in 10 different LSMs. Their results document that parameters associated with soil properties appear to play a more significant role than those associated with vegetation properties whereas the outputs of the diverse models considered exhibit the highest sensitivity to the maximum soil moisture content, considering three different hydroclimatic scenarios. Bastidas et al. (2006) assess parameter sensitivity of 5 different LSMs with increasing level of complexity in the description of vegetation-related physical processes. These authors show that (*i*) the sensitivity of the energy budget component to parameters with similar physical meaning employed in the diverse LSMs analyzed depends on the specific LSM model and varies depending on the location of the system, and (*ii*) soil-related parameters could be considered as most influential. Based on the hydrologic model WetSpa (Wang et al., 1996), Yang et al. (2012) highlight a strong sensitivity of runoff flow rate of two water catchments to parameters involved in the description of the evapotranspiration process. Li et al. (2013) employ diverse sensitivity analysis methodologies to assess sensitivity of 6 model outputs of the LSM CoLM (Dai et al., 2003), i.e., sensible heat, latent heat, upward longwave radiation, net radiation, soil temperature, and soil moisture, with respect to 40 uncertain model parameters. Their results highlight that all model outputs are sensitive to the Clapp and Hornberger parameter (which is related to soil water retention; see Clapp and Hornberger, 1978). Otherwise, (*i*) aerodynamic roughness length markedly influences the sensible and latent heat fluxes (along with the upward longwave and net radiations and soil temperature) and (*ii*) soil porosity chiefly governs soil moisture. Li et al. (2013) suggest that latent heat flux (related to evapotranspiration) is also sensitive to quantum efficiency of vegetation photosynthesis and minimum soil suction. Baroni and Tarantola (2013) employ classical variance-based Sobol indices to rank the importance of model parameters and forcing terms involved in the simulation of the mean soil moisture of the root zone, the cumulative evaporation, and the water flux below the root zone upon leveraging on the SWAP model (van Dam et al., 2008). Their results suggest that uncertainty related to the crop parameters (i.e., crop height, root depth, and the Leaf Area Index (*LAI*)) does not have a significant effect on these three model outputs in the setting analysed. Maina and Siirila-Woodburn (2020) evidence a marked sensitivity of evapotranspiration to soil parameters across the vadose zone, transpiration being otherwise mostly controlled by saturated soil parameters. On the other hand, Tafasca et al. (2020) report a weak sensitivity to diverse spatial maps of soil types and properties in the context of their analysis of water budget at the global scale. Saqr et al. (2021) rely on sensitivity analysis to identify the key factors influencing a geographic information system-based multi-criteria decision analysis targeting the exploitation of groundwater in the Wadi El-Natrun basin (Egypt). Their result document the importance of the distance from the aquifer-feeding fault, the aquifer hydraulic conductivity and the land surface elevation in controlling over-exploitation of the groundwater resource. Sobol indices estimated through a surrogate model are also used by Maina et al. (2022) to highlight the significant impacts of hydrodynamic parameters' uncertainties on simulated evapotranspiration. These Authors show that, under energy limited conditions and where plants have access to groundwater, uncertainty on evapotranspiration is related to uncertainties in saturated hydraulic conductivities. Under water limited conditions, the parameters that contribute to evaporation uncertainty are those related to unsaturated flow conditions.

The above-mentioned studies represent only a subset of the extensive literature on diagnosis of LSMs through sensitivity analyses. Nevertheless, they consistently highlight that the importance of model parameters may vary depending on several factors. These include the specific model output of interest, the processes embedded in the employed LSM, the prevailing hydroclimatic conditions, and possibly the selected sensitivity analysis methodology and ensuing metrics. Thus, additional investigations are required to fill this fundamental knowledge gap and enhance our ability to fully diagnose and understand the way complex LSMs function. In this sense, it is important to assess the sensitivity of various hydrological outputs to diverse model parameters under varying conditions (such as, e.g., vegetation types or seasonal settings) while applying multiple sensitivity analysis approaches to strengthen the reliability of results and our confidence in interpreting these.

In this context, this work aims at providing a comprehensive sensitivity analysis across spatial and temporal locations within a hydrological system to highlight the most relevant model parameters and the corresponding processes that need to be considered in a LSM. Here, we rely on a modular LSM developed at the Institut Terre et Environment de Strasbourg (ITES – Strasbourg Earth and Environment Institute) to simulate key components of the water cycle and to assess their sensitivity with respect to diverse model parameters that are typically affected by uncertainty. As target outputs, we consider actual evaporation, actual transpiration and groundwater recharge. Our study is anchored on field conditions (in terms of, e.g., climate, vegetation, and soil type) associated with two watersheds in the Vosges region (France) and documented across a one-year period. Runoff is not considered in this work, since its contribution to the water balance is documented to be negligible under our meteorological and field conditions (i.e., rain of low intensity, permeable soil mainly covered by forests). We set our sensitivity analysis study in an *ab initio* context. In this sense, uncertainty in the LSM parameters is linked a to our a priori (e.g., derived from prior experience and/or literature information) knowledge of the two watersheds properties and conditions. We emphasize that an *ab initio* sensitivity analysis strategy of the kind we pursue is primarily aimed at enhancing our knowledge of model dynamics by (*i*) identifying uninfluential parameters and (*ii*) identifying spatial and temporal intervals across which there is high sensitivity. Furthermore, to enrich our investigation of LSM dynamics, our detailed sensitivity analysis considers four diverse sensitivity indices: (*i*) the distribution-based Borgonovo index (Borgonovo, 2007); (*ii*) the variance-based Sobol indices (Sobol, 2001); and (*iii*) the moment-based *AMAE* and *AMAV* indices (Dell'Oca et al., 2017). The relevance of relying on various sensitivity analysis, each providing a unique contribution to enriching our understanding of system behavior, is underlined in several studies (e.g., Li et al., 2013, Maina and Guadagnini, 2018; Bianchi Janetti et al., 2019; Ju et al., 2021; Sandoval et al., 2022; and references therein). Thus, our

study contributes to the growing body of research focused on diagnosis and understanding of LSM behavior upon offering a comprehensive assessment grounded on synergistic integration of multiple sensitivity analysis methods applied across varying spatial and temporal scales within a hydrological system. This framework enhances the robustness of results (such as identifying the most influential parameters) and at the same time provides new insights into the functioning of LSMs under diverse environmental conditions.

Importance of model parameters is identified through a global sensitivity analysis in an *ab initio* context, i.e., the degree of uncertainty assigned to the vegetation and soil model parameters is grounded on a priori qualitative knowledge (e.g., prior experience, literature data) associated with the investigated sites and hydrological settings. We note that our study is not tailored to evaluating parameter uncertainty based on a model calibration procedure against experimental data associated with the modeled system (e.g., measured transpiration fluxes) and the way such (constrained) uncertainty propagates onto model outputs.

The methodological aspects associated with the LSM development and implementation, the definition of the various sensitivity indices, and the description of the hydrological settings associated with the catchments are presented in Section 2. Modeling results and the ensuing sensitivity analyses are illustrated in Section 3, while conclusions are drawn in Section 4.

2. Methodology

2.1. NIHM modular land surface model

NIHM Modular Land Surface model (NIHM-MLSM) is a companion of the hydrological model NIHM (Normally Integrated Hydrological Model – see Pan et al. (2015) and Jeannot et al. (2018)). NIHM-MLSM is a one-dimensional (along the vertical) model designed to compute on an hourly basis (*i*) the energy balance at the soil and vegetation level, as well as (*ii*) the water balance from the top of the vegetation layer to the groundwater table. Diverse mathematical formulations for processes such as transpiration, evaporation, and snow melt can be selected in conjunction with a modular structure on the basis of the observation that (*a*) application of a unique model formulation across different soil and vegetation types is questionable (Hogue et al., 2006) and (*b*) this allows adaptation to system complexity (Fisher and Koven, 2020).

Details of NIHM-MLSM are provided in the supplementary material. Here, we recall only the main mathematical formulations, assumptions, and parametrization.

2.1.1. Energy balance

The model concepts draw from the theory of Shuttleworth and Wallace (1985) for sparse-crop evaporation. Similar concepts have been used by, e.g., Braud et al. (1995) and Boulet et al. (2015).

The system consists of two surfaces, i.e., the cover and the ground below cover.

The energy balance at the ground surface is given by:

$$R_n^g = H_g + \rho_w \lambda E_g + G + \rho_w \lambda_f Q_{Sm} \tag{1}$$

At the cover surface, it reads:

$$R_n^c = H_c + \rho_w \lambda E_c \tag{2}$$

The continuity of the sensible and latent heat fluxes is added to the two balance equations:

$$\begin{cases} H = H_g + H_c \\ \rho_w \lambda E = \rho_w \lambda E_g + \rho_w \lambda E_c \end{cases} \tag{3}$$

Here, R_n^g and R_n^c correspond to the net radiation reaching the ground and cover surfaces (W/m^2), respectively; H_g and H_c denote surface sensible heat flux at the ground and cover surface (W/m^2), respectively; and $\rho_w \lambda E_g$ and $\rho_w \lambda E_c$ denote the soil and cover surface latent heat flux (W/m^2), respectively.

Main assumptions related to the formulation of the energy balance comprise the following:

- steady-state is considered, upon assuming that vegetation and soil layers have negligible heat capacity;
- conductive heat fluxes are expressed on the basis of a resistance analogy, similar to Ohm's law;
- the amount of energy absorbed by the vegetation and received by the ground are estimated by assuming a Beer-Lambert transmission reflectivity through the vegetation (Deardorff, 1978; Taconet et al., 1986) and depend on the leaf area index (*LAI*) and an attenuation coefficient;
- transpiration takes place only in the canopy; stomatal conductance is evaluated using a Jarvis-type multiplicative model (Cox et al., 1998; Jarvis, 1976) and is affected by the environmental factors embedded in the efficiency functions (solar radiation, air temperature, vapor pressure deficit); the *LAI* is used to scale stomatal conductance to canopy conductance;
- water intercepted by the canopy is assumed to evaporate with negligible impact on energy balance (Kergoat, 1998);
- the soil heat flux is approximated as proportional to the net radiation (Clothier et al., 1986; Choudhury and Monteith, 1988; Kustas and Daughtry, 1990).

The numerical strategy used to solve the four equations listed above is detailed in the supplementary material.

2.1.2. Water flow and balance

Water balance is formulated for three diverse compartments, i.e., the canopy, the snow cover, and the soil. Key concepts associated with the water balance model for the canopy are: (*i*) water from precipitation is partly stored in the canopy, whose storage capacity is limited to a maximum value; (*ii*) the intercepted water is subject to evaporation and does not contribute to throughfall (i.e., the process according to which excess water leaves wet leaves to reach the ground surface); (*iii*) surface runoff is neglected, thus assuming that the rate at which water reaches the ground does not exceed soil infiltration capacity (as a result, no significant ponding and/or runoff take place).

The snow model is adapted from the snow module of the HBV hydrological model (Seibert and Bergström, 2022; Seibert and Vis, 2012). It consists in splitting precipitation (after interception) in either snow, rain, or both. A conceptual model based on snowpack temperature is used to estimate snowmelt fluxes (Neitsch et al., 2002).

Flow in the unsaturated zone is described by introducing three types of reservoirs (or layers): (*i*) the litter, corresponding to the layer in contact with the atmosphere and where only evaporation takes place; (*ii*) the root zone, which is colonized by plant roots and supplies water for transpiration; and (*iii*) a set of sequential reservoirs to mimic vertical water movement below the root zone down to the groundwater table. Each reservoir is defined through a given water content at saturation, the water content at wilting point (which is also considered as the residual water content), and water content at field capacity.

Water from throughfall and melted snow infiltrates in the litter layer. Evaporation (as computed by energy balance at the soil surface) occurs only in this layer, and the amount of evaporated water is linearly related to water content. Water drained from the litter layer enters the root layer. Transpiration (estimated with the energy balance for the canopy) takes place only in this layer, and its amount is adapted according to the available water therein. Drainage from the different layers is estimated in two ways: (*i*) the water volume above the layer field capacity is drained immediately to the next layer, to represent water movement due to gravity; and (*ii*) when water content lies between the field capacity and the wilting point (i.e., residual water content), drainage is computed as an exponential function of the available water amount.

2.2. Global sensitivity analysis

A critical step in diagnosing and understanding the functioning of a model involves quantifying the relevance that different uncertain model parameters exert on model results of interest. This allows identifying (possible) influential and non-influential parameter sets. These are here assessed through global sensitivity analysis. In broad terms, the latter enables one to quantify the (relative) strength of the influence of the variability/uncertainty in a given parameter on the corresponding variability/uncertainty in the output(s) of the model analyzed.

Our study rests on two complementary global sensitivity analysis methodologies: (*i*) density function- and (*ii*) and moment-based strategies. While the former is tailored to analyze the effects that variations of uncertain model parameters have on the whole (probability or cumulative) density function of the model output, the latter focuses on the impact on given statistical moments of the density function of model output. The combination of both strategies yields a more comprehensive understanding of parameter influence on model output uncertainty. This approach captures different facets of uncertainty, making it possible to identify parameters that affect either the overall shape of the output distribution or its key statistical features. In our analysis, we consider the Borgonovo index (Borgonovo, 2007) as a density function-based metric. For moment-based metrics, we use the Sobol indices (Sobol, 2001) along with the *AMAE* and *AMAV* indices proposed by Dell'Oca et al. (2017). These indices are widely used in environmental system modeling due to their straightforward interpretability and ability to reveal different aspects of model sensitivity and behavior. All selected metrics are suitable for models with nonlinear formulations and can be applied under both uncorrelated and correlated parameter settings. Otherwise, it is noted that accurately quantifying the effect of parameter correlations on sensitivity still remains an open challenge. In this study, we assume parameter independence. This choice is based on the exploratory nature of our work and the lack of a clear and strong evidence for significant parameter correlations.

Considering $\boldsymbol{X}$ as a set of random independent parameters and Y as the corresponding model output, the Borgonovo index (B) associated with parameter X_i is defined as:

$$B_{X_i} = \frac{1}{2}\int f_{X_i}(x_i)\left[\int \left|f_Y(y) - f_{Y|X_i}(y)\right| dy\right] dx_i \tag{4}$$

Here, $f_{X_i}(x_i)$ is the marginal probability density function (pdf) of the i-th model (input) parameter X_i; $f_Y(y)$ and $f_{Y|X_i}(y)$ are the unconditional and conditional (to a given value of X_i) marginal pdf of Y, respectively. Note that the Borgonovo index grounds the concept of the sensitivity of Y to X_i on the base of the (average) distance between the unconditional pdf of the output and its counterparts stemming from conditioning on diverse (plausible) values of X_i. This index ranges in the unit interval, where a null value corresponds to scenario in which the pdf of Y is unaffected by variations in parameter X_i.

We also rely on the classical Sobol indices (Sobol, 2001) to quantify the contribution of the uncertainty in X_i to the model output variance when considered alone, i.e., principal index SP_{X_i}, or as it interacts with other parameters, i.e., total index ST_{X_i}. The principal Sobol index associated with X_i is given by:

$$SP_{X_i} = \frac{V[E[y|X_i]]}{V[y]} \tag{5}$$

where E[-] and V[-] denote the expectation and variance operators, respectively, and $E[y|X_i]$ is the expected value of Y conditional to a particular value of X_i. The principal Sobol index measures the relative contribution of X_i to the model output variance without considering interactions with other uncertain model parameters. The corresponding total Sobol index embeds also the contributions of interactions with the remaining model parameters and is defined as:

$$ST_{X_i} = SP_{X_i} + \sum_{x_j} SP_{X_i,X_j} + \sum_{x_j,x_k} SP_{X_i,X_j,X_k} + \ldots \tag{6}$$

where SP_{X_i,X_j} is the fraction of model output variance due to the interactions between parameters X_i and X_j (the remaining symbols being characterized by a corresponding meaning). We recall that the total Sobol index represents the expected contribution of X_i to the variance of the model output, including contributions caused by its interactions with other input variables. Sobol indices are broadly used because of their simplicity and intuitive nature to assess sensitivity of models to input parameters by decomposing the total variance of a model output of interest into different contributions, each associated with a subset of parameters. These indices are used to measure the importance of individual parameters and interactions between parameters (Sobol, 2001).

To complement our investigation, we evaluate the moment-based metric introduced by Dell'Oca et al. (2017), termed *AMA* indices. The latter quantify sensitivity as the degree of variations in given statistical moments of the target model output Y that are due to the variability in model parameter X_i. Considering the expected value of Y, we introduce the following moment-based index:

$$AMAE_{X_i} = \begin{cases} E\left[\left|y_0 - E[y|X_i]\right|\right]/\left|y_0\right| & y_0 \neq 0 \\ E\left[\left|E[y|X_i]\right|\right] & y_0 = 0 \end{cases} \tag{7}$$

where y_0 is the unconditional expected value of Y. Considering the second (centred) statistical moment, i.e., the variance of Y, we introduce following index:

$$AMAV_{X_i} = E\left[\left|V[y] - V[y|X_i]\right|\right]/V[y] \tag{8}$$

Relying on the *AMA* indices enables one to assess the sensitivity of Y in terms of various salient features of the probability density function of the target model output, as rendered through diverse statistical moments. Here, we focus on the mean and the variance of the model output. These metrics have been applied in diverse settings, including scenarios related to, e.g., groundwater hydrology (Bianchi Janetti et al., 2019; Dell'Oca, 2023), subsurface energy resources associated with gas flow migration across low-permeability media (Sandoval et al., 2022), analysis of seismic metabarriers (Zeighami et al., 2023), dynamics of emerging contaminants in groundwater (Ceresa et al., 2023), or assessment of infiltration structures (Dell'Oca et al., 2023b).

Our reliance on various sensitivity indices is in line with the observation that it is often difficult for one method to provide a complete sensitivity assessment. This is even more critical for complex hydrological systems of the kind we consider here (Mai et al., 2022).

2.3. Study catchments and data-sets

The NIHM-MLSM model is run under field conditions (in terms of climate, vegetation, and soil type) on two catchments in the Vosges region of northeastern France (i.e., in the Bruche and Doller catchments – see Fig. 1 in the supplementary material (SM)) that are characterized by similar climatic conditions while being associated with differing soil types and vegetation. While the model is run in a distributed way on the whole extent of each catchment, results are only illustrated for a selected location (or computational pixel of size 200x200m^2) for each catchment, for simplicity.

Each pixel is selected based on its representativeness of the corresponding catchment conditions, including soil type, climate, and vegetation cover. Within each catchment, these characteristics are associated with a high degree of spatial homogeneity, thus allowing a single pixel to serve as a proxy for the broader area. Both locations are subject to an oceanic climate, being affected by continental traits (Peel et al., 2007) due to the action of Foehn. Consequently, considerable fluctuations in local climatic variables, such as air temperature or rainfall rates, are experienced. Historical streamflow data indicate a low-water period

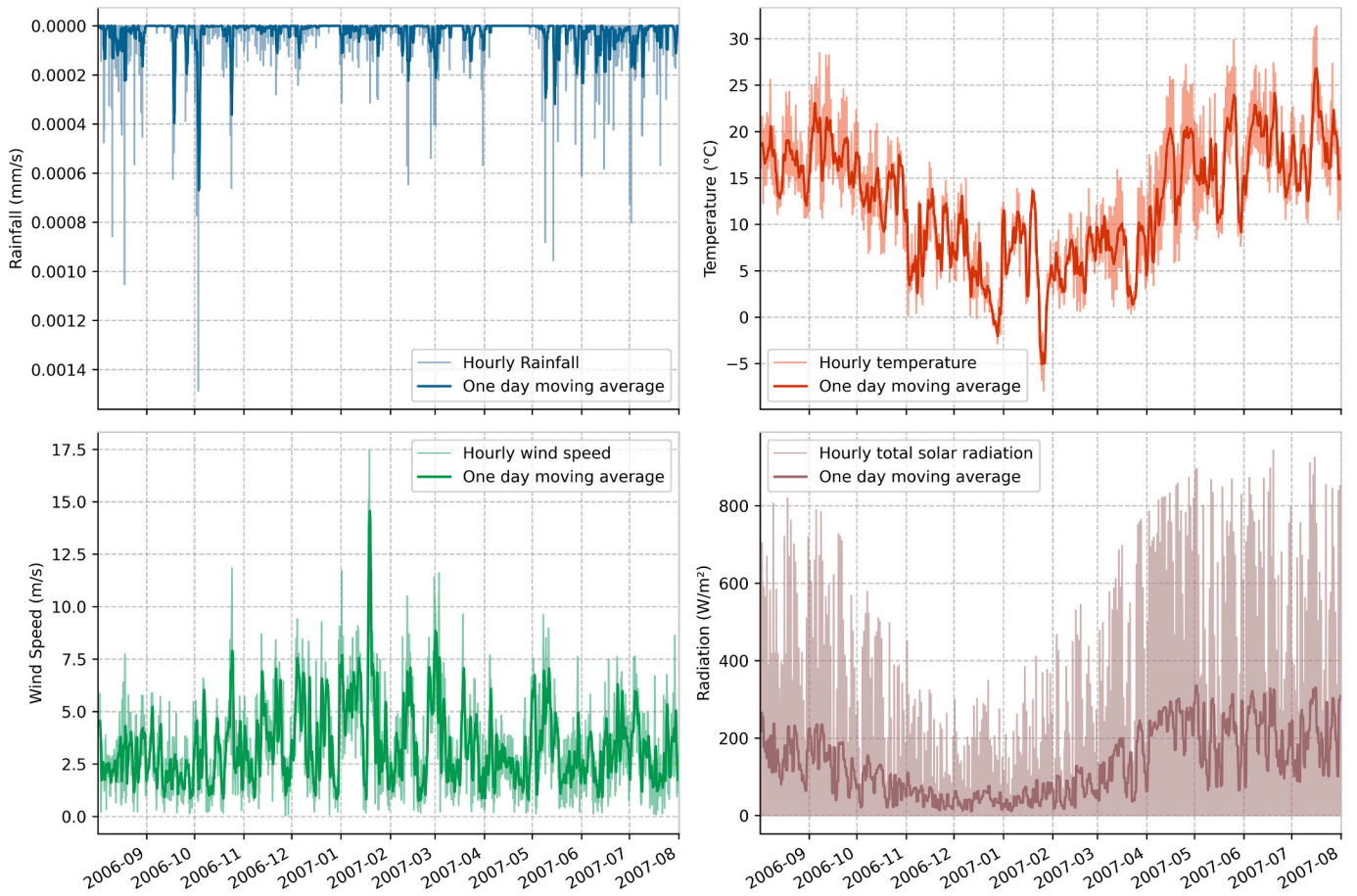

Fig. 1. Main climatic forcing for the Bruche watershed, i.e., rainfall, air temperature, wind speed and solar radiation. Hourly values (light color) and their daily moving averaged counterpart (darker color) are depicted.

taking place between June and October and a high-water period between December and March (Banque HYDRO, 2020).

The first exemplary location considered in this study is located in the Bruche catchment, which is characterized only by vineyards on Calcosol soil. The second location considered is representative of the Doller catchment, which is covered by deciduous forest, moorland and heathland in combination with the Alocrisols soil. Figs. 1 and 2 depict records of the main climatic forcings monitored across the study period, i.e., precipitation, temperature, wind speed, and solar radiation reaching the canopy for the Bruche and Doller watersheds, respectively.

Climatic data (air temperature, air humidity, precipitation, snow, wind speed, incoming solar radiation, and longwave radiation) are included in the Safran database produced by Météo-France (Durand et al., 1993; Habets et al., 2008). The Safran system provides values of key climatic variables interpolared from ground measurements on a fixed grid of $8 \times 8\ km^2$ with a hourly temporal resolution (Durand et al., 2009; Quintana-Seguí et al., 2008). It has been widely used to address hydrological monitoring and climate change studies (Vidal et al., 2010). Note that uncertainty on these forcing terms is not considered in this work which is otherwise specifically focused on the parameters required for LSMs.

Similar to other LSMs, NIHM-LSM requires the estimation of numerous forcing terms and parameters related to climatic conditions, vegetation and soil characteristics. Several factors limit our ability to obtain a reliable estimate of these forcing terms and parameters. These include, e.g., incompatibility between the model scale and the support volume of the measurement and the inherent space and time variability of most of the parameters that makes the exhaustive knowledge of model parameters and forcing terms as practically unfeasible. Therefore, identification of the parameters that can be considered as most important to given model outputs is critical to effectively assist modeling and estimation of land surface energy and water fluxes. Note that we consider as important (or influential) those model parameters whose variations impact to some extent model outputs of interest, i.e., transpiration, evaporation and groundwater recharge fluxes in this study. Such parameters are identified through a global sensitivity analysis in an ab initio context, i.e., the degree of uncertainty assigned to the vegetation and soil model parameters is grounded on a priori qualitative knowledges (e.g., prior experience, literature data). In the present study, we do not evaluate parameter uncertainty based on a model calibration procedure against experimental data associated with the modeled system (e.g., measured transpiration fluxes).

In this study, the uncertain parameters involved in the evaluation of transpiration, evaporation, and groundwater recharge fluxes at a given time are:

- the *LAI* and the albedo; considering their smooth variation over time, we rely on linearly interpolated monthly data; this implies that a given simulation moment is associated with two *LAI* and two albedo parameter values;
- five parameters for the litter layer (i.e., residual water content, field capacity, porosity, thickness, and drainage coefficient) and four parameters for the root layer (residual water content, field capacity, porosity, and drainage coefficient) per soil type. Root layer thickness is considered as a vegetation dependent parameter through the root depth.

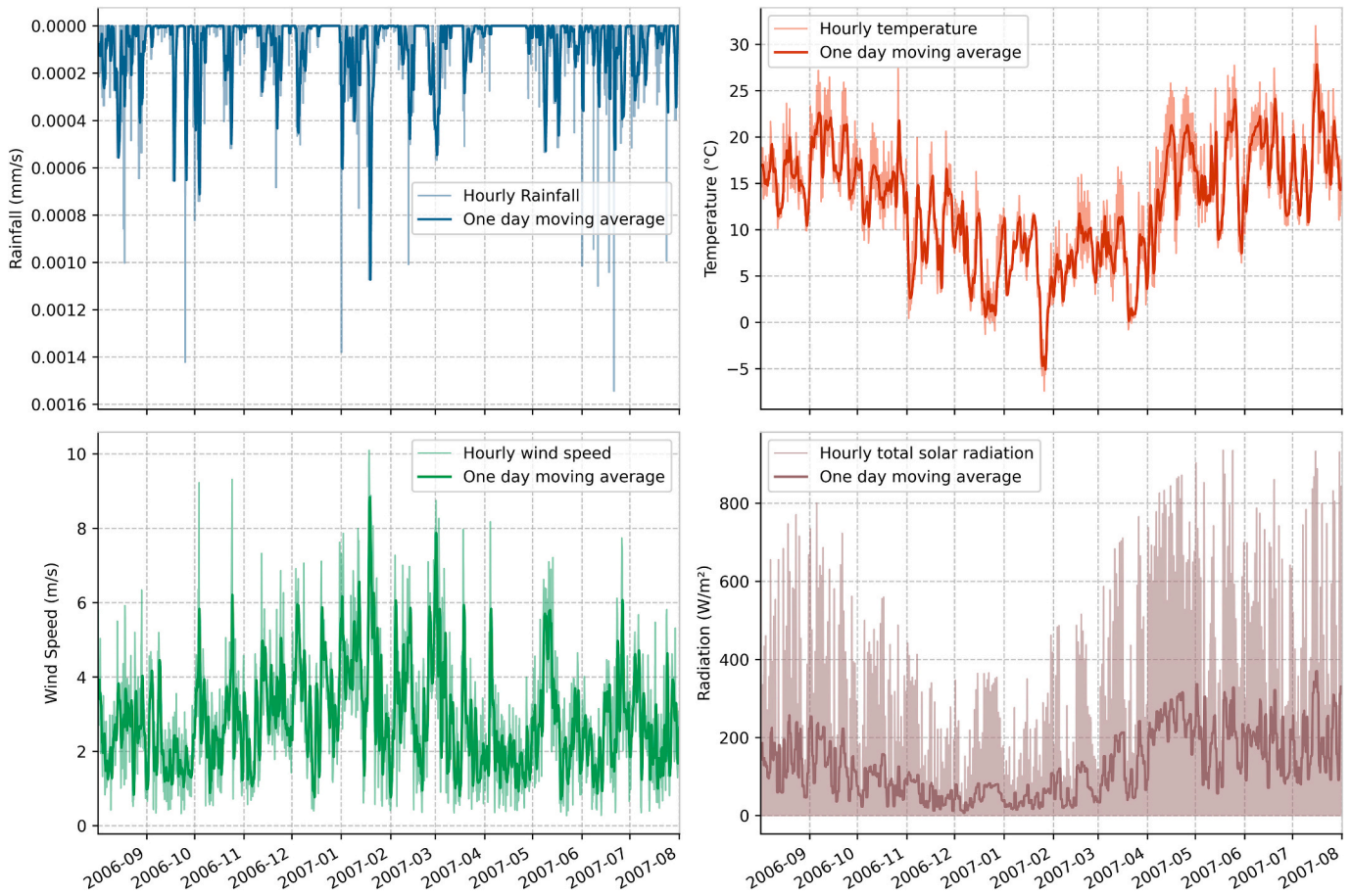

Fig. 2. Main climatic forcing for the Doller watershed, i.e., rainfall, air temperature, wind speed and solar radiation. Hourly values (light color) and their daily moving averaged counterpart (darker color) are depicted.

- five vegetation-related parameters per vegetation type (i.e., precipitation interception, radiation attenuation, root depth, stomatal conductance, and canopy height);

A total number of 16 parameters is associated with a given type of vegetation and a given type of soil.

Monthly values for *LAI* (Table 1) are estimated from satellite data at a spatial scale of 3×3 km^2 (downloaded from https://land.copernicus.eu/global/products/ (Copernicus Climate Change Service, 2018)). When several values are associated with a given month, we consider their average as a representative monthly value. If only one value is available, it is then considered as the average value across the month.

Albedo values rendered by the satellite information downloaded from the Copernicus Climate Change Service (2018) were found very uncertain. The albedo of the canopy is given by the formulation provided by Planque (2018), who estimated albedo values of numerous forests located across France. The formulation is:

$$\alpha_c = 0.18 + Z \times 0.02 \quad (9)$$

Here, Z is a random number uniformly distributed over [-1; 1]. The soil albedo is set equal to 0.10 (Van Wijk and Scholte Ubing, 1963).

The Corine Land Cover database (https://land.copernicus.eu/en/products/corine-land-cover) allows for the identification of distinct vegetation categories at each studied catchment at raster scale of 100 m (European Union - SOeS, 2018). Table 2 lists the support (i.e., ranges of variability) associated with the uncertain vegetation-related parameters for the diverse vegetation types related to the two watersheds here considered. The width of these supports is identified on the basis of a detailed analysis of previous literature studies. For completeness, we list the main literature sources analyzed for each vegetation-related parameter:

- precipitation interception (Brecciaroli et al., 2012; Couturier and Ripley, 1973; Friesen and Van Stan, 2019; Kergoat, 1998; Nicholas et al., 2011);
- radiation attenuation coefficient (Zhang et al., 2014);

Table 1
Monthly values of *LAI* (mean and standard deviation, denoted as St Dev) for the pixel located in the Bruche and the Doller catchments.

Month	1	2	3	4	5	6	7	8	9	10	11	12
	Bruche catchment											
Mean	1.10	0.87	1.37	2.97	2.03	2.20	4.20	2.83	2.17	0.50	1.07	0.86
St Dev	0.06	0.05	0.05	0.05	0.05	0.05	0.05	0.05	0.05	0.04	0.06	0.08
	Doller Catchment											
Mean	1.09	0.80	1.17	1.73	4.80	5.67	5.80	5.40	5.27	4.57	1.23	0.86
St Dev	0.06	0.05	0.05	0.05	0.05	0.05	0.05	0.05	0.05	0.06	0.06	0.07

Table 2
Vegetation-dependent parameters (minimum and maximum values) for **T1:** Vineyards (Bruche catchment), **T2:** Deciduous forests (Doller catchment) and **T3:** Grasslands, Natural grasslands and pastures, Moors and heathland (Doller catchment).

Vegetation type	Interception [-]		Attenuation [-]		Root Depth [m]		Stomatal conductance [m/s]		Canopy height [m]	
T1	0.02	0.06	0.16	0.54	0.5	2.5	0.005	0.015	0.2	1.2
T2	0.04	0.08	0.29	0.65	0.6	2.3	0.0002	0.0036	12.6	27.0
T3	0.04	0.08	0.35	0.65	0.2	1.0	0.0011	0.0110	0.2	2.1

- root depths (Escamilla et al., 1991; Freeling and Walbot, 1994; Leuschner et al., 2001; Mueller et al., 2013; Richards, 2011; Grassland: Mission: Biomes, 2023);
- stomatal conductance (Gowdy et al., 2022; Brewer et al., 2022; Carter, 1998; Charreyron, 2011; Hovenden and Brodribb, 2000; Jonard et al., 2011; Baca Cabrera, 2021; Kim and Verma, 1991; Mahhou et al., 2005; Mueller et al., 2013; Ocheltree et al., 2012; Reis and Ribeiro, 2020; Song et al., 2018; Tardieu et al., 1991; Winkel and Rambal, 1993; Zhang et al., 2012);
- canopy height (Campos et al., 2021; Liu et al., 2019; Matese et al., 2017; Grassland: Mission: Biomes, 2023; Peiffer et al., 2014; Smirnova et al., 2008).

Only the vineyards vegetation is considered (T1 in Table 2) at the Bruche catchment. Two types of vegetation are considered for the location selected at the Doller catchment. These correspond to (*i*) vegetation composed mainly of broad-leaved species, including shrub and bush understoreys for 2/3 of the pixel area (T2 in Table 2) and (*ii*) vegetation resulting mainly from forest degradation (low and closed cover, dominated by bushes, shrubs and herbaceous plants) for 1/3 of the pixel area (T3 in Table 2).

Soil types are classified upon relying on the Regional Soil Reference System for Alsace and Vosges (https://data.europa.eu/data/datasets/fr-341142131-araa_bdsol-alsace_250000_2011?locale=fr). Six main categories are identified (Chambre Régionale d'Agriculture Grand Est, 2011, 2015) and denoted according to the World Reference Base for Soil Resources (IUSS Working Group WRB, 2022).In this work we consider only the first two soil layers (i.e., litter and root zone) and groundwater recharge is assumed to coincide with drainage from the root zone, the overall thickness of the unsaturated zone being limited to a few meters. Table 3 lists ranges of variability associated with the uncertain soil-related parameters for the diverse soil types of interest. As stated above, the width of these supports is set on the basis of previous studies (Belfort et al., 2018; Clapp and Hornberger, 1978; Dingman, 2002). Note that soil types S1 and S2 constitute typical traits of the Bruche and Doller catchment, respectively.

Drainage coefficients for both layers and all soil types are set to range between 5.0×10^{-8} and 5.0×10^{-7} [-]. This range of variability has been defined on the basis of the temporal pattern of groundwater recharge fluxes obtained through preliminary model runs (details not shown). Residual water content is fixed at 0.01 for all soil types. We further note that, since a single pixel is used to represent each catchment, the prescribed parameter uncertainty ranges for soil and vegetation types also serve to account for the potential heterogeneity of these attributes within the catchment area.

Evaluation of the global sensitivity indices listed in Section 2.2 is performed through a numerical Monte Carlo (MC) approach. Parameter values are randomly sampled by considering model parameters as independent and identically distributed random variables, each characterized through a uniform distribution with support given in Tables 2 and 3. With reference to *LAI* and albedo, the semi-width of the support is set to the value of the standard deviation provided in the Copernicus data sets.

Sobol indices are calculated upon considering the algorithm described in Saltelli (2007). A total of 90,000 simulations are performed for each of the catchments.

The temporal window associated with our simulations spans a period of two years (i.e., 01/08/2005 to 31/07/2007). The analyses target solely the second year of simulations, to minimize impacts of initial conditions on model outputs.

3. Results and analysis of average water fluxes

Here, we illustrate the type of results obtained with the modeling study to assist grasping the overall behavior of the systems and to provide a first quantitative appraisal of the nature of the available observations and modeling outputs related to the complex hydrological systems analyzed. We rely on graphical depictions rendered in terms of the expected value +/- one standard deviation of daily averaged values grounded on the set of MC simulations for the period from August 1st, 2006 to July 31th, 2007. Temporal dynamics of actual evaporation, transpiration, and groundwater recharge fluxes (as evaluated through the NIHM-MLSM model) are provided in Figs. 3 and 4 for the selected locations in the two watersheds (see Section 2.3), together with the corresponding observed rainfall series. Detailed quantitative results concerning the main components of the water cycle are listed in Table 4 and 5 for the pixel located in the Bruche and Doller catchments, respectively.

We enhance our analysis by comparing potential and actual evaporation and transpiration fluxes at the Bruche and Doller catchments, as shown in Figs. 5 and 6, respectively. Potential transpiration and evaporation fluxes are derived by solving the energy balance model, which primarily depends on the available energy input and is slightly adjusted by the efficiency function governing stomatal transpiration. In contrast, actual evaporation and transpiration fluxes are related to potential fluxes but are constrained by water availability (specifically, in the litter layer for evaporation and in the root zone for transpiration).

Although the watersheds are geographically close, their precipitation patterns differ significantly. Tables 4 and 5 show that the annual precipitation amounts vary greatly between the two catchments, with 903 mm recorded for the Bruche and 2542 mm for the Doller. Additionally, during winter, the Bruche catchment receives relatively little precipitation (18 % of the annual total), whereas the Doller catchment experiences substantial precipitation events (31 % of the annual total). These findings are further supported by the analysis of rainfall events depicted in Fig. 3a and Fig. 4a.

Table 3
Soil-dependent parameters (minimum and maximum values) for **S1:** Calcosols and Calcisols (Bruche catchment) and **S2:** Alocrisols (Doller catchment).

Soil	**Root layer**				**Litter layer**					
Type	**Field capacity θ_c [-]**		**Porosity θ_s [-]**		**Field capacity θ_c [-]**		**Porosity θ_s [-]**		**Thickness (m)**	
S1	0.22	0.33	0.42	0.48	0.25	0.35	0.50	0.80	0.05	0.15
S2	0.12	0.16	0.40	0.45	0.17	0.25	0.50	0.80	0.05	0.15

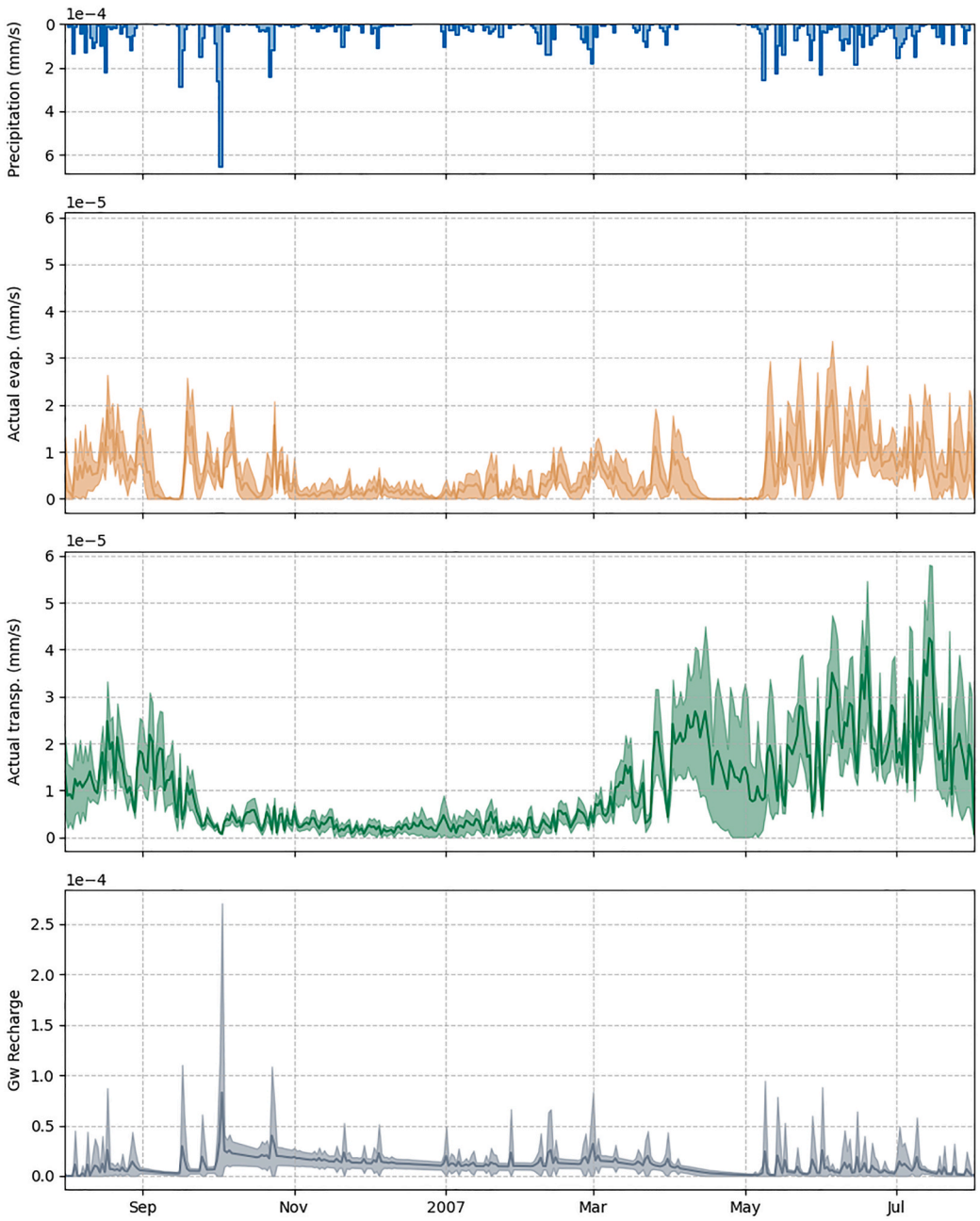

Fig. 3. (a) Observed precipitation and values of (b) evaporation and (c) transpiration together with (c) groundwater recharge evaluated through the NIHM-MLSM model at the Bruche watershed. Solid curves and shaded areas in (b)-(c) correspond expected values and +/- one standard deviation of daily averaged values grounded on the set of MC simulations for the period from August 1st, 2006 to July 31th, 2007, respectively. Note the different scales for recharge and rain.

Tables 4 and 5 indicate that the total annual evaporation at the Doller catchment is approximately twice the one at the Bruche catchment. However, percentage contributions of evaporation to the annual total exhibit similar seasonal trends across both catchments. This observation aligns with the patterns shown in Fig. 3b and Fig. 4b. During the spring and summer seasons, evaporation remains relatively stable at both Bruche and Doller, fluctuating around a nearly constant value. Figs. 5 and 6 reveal that potential and actual transpiration values are closely aligned at both catchments during the spring and summer seasons, indicating energy-limited regimes. In contrast, the fall and winter seasons reveal differing dynamics between the two sites. At Bruche, precipitation during the typically dry-soil period of fall and winter is less abundant and more sporadic. Consequently, evaporation is generally low during this time, with variations closely following rain events. Evaporation rates at Bruche tend to peak shortly after precipitation events (notably in October and March, when more energy is available) and then decline due to limited water availability. Fig. 5 reveals that at Bruche actual transpiration is generally water-limited. Conversely, precipitation at the Doller catchment during fall and winter is more intense and frequent, leading to generally wetter soil conditions. These conditions sustain higher evaporation rates that stabilize over multi-week periods (e.g., late September to October, late November, February, and early March) following substantial rainfall. Nonetheless, these periods are followed by sharp declines in evaporation to low or near-zero levels, reflecting the depletion of water resources. Additionally, low evaporation rates coincide with extended dry periods without rain, as shown in Fig. 3a and b Fig. 6 corroborates the switch of the transpiration dynamics at Doller during the fall-winter period from being energy or water-limited in response to the series of rain events. Overall, this set of results indicate the relevance of water-availability in

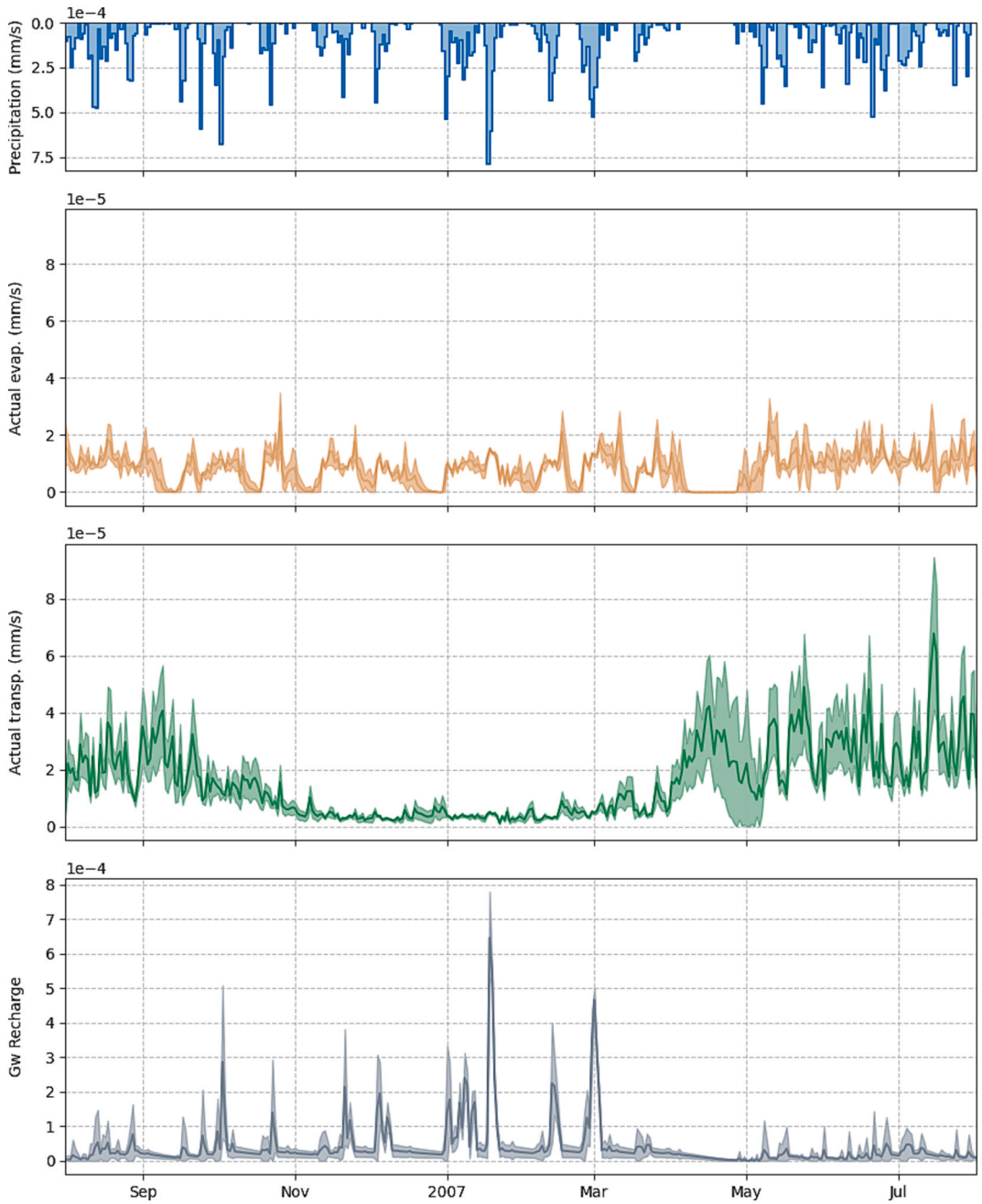

Fig. 4. (a) Observed precipitation and values of (b) evaporation and (c) transpiration together with (c) groundwater recharge evaluated through the NIHM-MLSM model at the Doller watershed. Solid curves and shaded areas in (b)-(c) correspond expected values and +/- one standard deviation of daily averaged values grounded on the set of MC simulations for the period from August 1st, 2006 to July 31th, 2007, respectively. Note the different scales for recharge and rain.

the litter layer (where transpiration takes place). Overall, these results highlight the critical role of water availability in the litter layer, where transpiration occurs. In addition to the series of precipitation events, key parameters influencing water availability in the litter layer include precipitation interception by the vegetation cover, storage capacity determined by the layer porosity and thickness, and the drainage rate. On the other hand, the seasonal fluctuations of radiation (see Figs. 1 and 2) seems to play a minor role in determining the values of potential transpiration (particularly at Doller). Nevertheless, radiation-filtering parameters associated with the canopy (e.g., height, radiation attenuation coefficient) can markedly influence the amount of energy available for transpiration.

An analysis of transpiration fluxes (see Tables 4 and 5) reveals a similar total amount of transpired water at the two catchments, despite differences in vegetation types and precipitation patterns. Furthermore, both catchments exhibit comparable seasonal contributions to total transpiration, as highlighted in Fig. 3c and Fig. 4c, with pronounced seasonal variability of transpiration fluxes, i.e., very low values recorded during fall and winter, contrasted by high rates during the vegetative seasons of spring and summer. The comparison of the evaporation and transpiration dynamics at both catchments suggests that seasonal variations in radiation have a much more pronounced effect on transpiration than on evaporation, while the characteristic of precipitation appears to have a minor influence. This suggests a dominance of an energy-limited regime for transpiration across the year at both sites. A notable exception is the very dry period in April, when transpiration becomes water-limited (note that transpiration at Bruche appears to be water-limited also in August). This set of observations is corroborated by the

Table 4
Amount of water volume (in mm) for the different seasons and over the year for the Bruche catchment. Values of transpiration, evaporation, and groundwater recharge are evaluated through the NIHM-MLSM model (mean ± standard deviation). Percentage values (%) are defined as the ratio between seasonal values and their yearly counterparts.

	Autumn	Winter	Spring	Summer	Total
Precipitation (mm)	213	165	238	288	903
(%)	*24*	*18*	*26*	*32*	*100*
Evaporation (mm)	26 ± 12	22 ± 13	50 ± 23	57 ± 24	154 ± 70
(%)	*17*	*14*	*32*	*37*	*100*
Transpiration (mm)	24 ± 7	32 ± 11	145 ± 50	133 ± 38	334 ± 101
(%)	*7*	*10*	*43*	*40*	*100*
GW Recharge (mm)	133 ± 34	100 ± 16	49 ± 46	45 ± 53	327 ± 134
(%)	*41*	*31*	*15*	*14*	*100*

Table 5
Amount of water volume (in mm) for the different seasons and over the year for the Doller catchment. Values of transpiration, evaporation, and groundwater recharge are evaluated through the NIHM-MLSM model (mean ± standard deviation). Percentage values (%) are defined as the ratio between seasonal values and their yearly counterparts.

	Autumn	Winter	Spring	Summer	Total
Precipitation (mm)	566	780	415	781	2542
(%)	*22*	*31*	*16*	*32*	*100*
Evaporation (mm)	65 ± 16	57 ± 11	80 ± 22	104 ± 22	306 ± 70
(%)	*21*	*19*	*26*	*34*	*100*
Transpiration (mm)	33 ± 9	43 ± 10	158 ± 47	148 ± 40	382 ± 104
(%)	*9*	*11*	*41*	*39*	*100*
GW Recharge (mm)	449 ± 33	612 ± 42	137 ± 56	299 ± 87	1497 ± 193
(%)	*30*	*41*	*9*	*20*	*100*

inspection of Figs. 5 and 6. Here, one can observe that: (*i*) close values of potential and actual transpiration are recorded across the whole year at both catchments; (*ii*) short mildly-dry periods have a more significant impact on actual evaporation than on actual transpiration as the latter is primarily driven by water availability in the root layer, which is buffered by drainage from the litter layer during dry periods; (*iii*) during the mid-weeks of April the impact of water limitations is more pronounced on the actual evaporation than on actual transpiration.

Regarding groundwater, Tables 4 and 5 reveal significant differences in total groundwater recharge between the two watersheds. At Bruche, approximately one-third of the total precipitation contributes to groundwater recharge, while this proportion increases to nearly half at Doller. These differences can be attributed to the varying precipitation levels across the catchments. Groundwater recharge primarily occurs during the fall and winter seasons at both catchments, accounting for over 35 % of the seasonal total. This is due to minimal competition for water from plants during these periods. However, the lower frequency of rainfall events at Bruche limits the intensity of groundwater recharge during fall and winter. Conversely, during spring and summer, groundwater recharge decreases across both catchments as water availability is primarily allocated to evaporation and transpiration processes.

Several parameters related to soil and vegetation characteristics are involved in the estimation of actual evaporation, transpiration fluxes, and the ensuing groundwater recharge. The results of the global sensitivity analysis presented in the next section allow identifying parameters that control these fluxes.

4. Results and assessment of model output variability in a sensitivity analysis context

Results from the Monte Carlo simulations can also be analyzed in terms of the ensuing pdf of an output of interest at a given time. Fig. 7 depicts exemplary pdfs obtained for diverse model outputs (i.e., (a) transpiration at Bruche, (b) evaporation at Doller, at different times) corresponding to unconditional scenarios (red curves) and settings that are conditional on diverse subintervals of variability for a given parameter. With reference to the latter element, we select here five equiprobable subintervals, for (a) root and (b) litter layer drainage coefficient. We recall that this type of visual depiction is akin to a regionalized sensitivity analysis. It assists one to grasp the impact that conditioning on diverse values (comprised within subintervals according to which the overall support is partitioned) of a parameter might have on the pdf of an output of interest.

Inspection of Fig. 7 reveals several interesting features. The pdfs of the transpiration rate (in terms of the ensuing (conditional) expected value, as well as other features, i.e., higher order statistical moments; see Fig. 7a) corresponding to on June 15th 2007 at 12 a.m. at Bruche appears to be sensitive to the root layer drainage coefficient. On the other hand, evaporation rate at Doller (see Fig. 7b) corresponding to October 6th 2006 at 1.p.m. appears to be insensitive to variations of the litter layer drainage coefficient with reference to all of the characteristic features of its pdf. These preliminary investigations for the diverse outputs and their response to model parameter variations suggest a complex behavior of the LSM here investigated. A detailed quantitative appraisal of sensitivity is illustrated in Section 3.2 on the basis of the metrics introduced in Section 2.2.

We evaluate the global sensitivity indices introduced in Section 2.2 on an hourly basis across a temporal window of one year. Fig. 8 depicts color-coded (from red/high to blue/low) values of B (Eq. (4)) ST (Eq. (6)), $AMAE$ (Eq. (7)), and $AMAV$ (Eq. (8)) indices for the evaporation rate at Bruche across the year and the diverse model parameters (listed along the vertical axis; corresponding parameter identification number (id) is defined in the Symbol List of the Supplementary Material). A light purple background highlights time-varying parameters (e.g., LAI: parameters 1–12; albedo: parameters 13–24), while a light green background indicates static parameters (e.g., soil: 25–38; vegetation cover 1: 39–43; vegetation cover 2: 44–48). a red band in the B index panel indicates a temporal window during which evaporation is highly sensitive (in terms of the full probability distribution) to a specific parameter. Inspection of the additional indices offer further insight into how the first and second moments of the output distribution respond to parameter variations. Taken together, results encapsulated in Fig. 8 allow for assessing consistency (or discrepancies) in parameter sensitivity depending on the specific aspect of the output distribution being analyzed. Figs. 10-13 are patterned after Figs. 8 and 9 considering the results for transpiration rate and groundwater recharge.

We recall that values of B (similar to all other indices) associated with parameters that are not influential to given model outputs of interest should be zero. For example, the value of B for the evaporation associated with the drainage coefficient of the root layer should be equal to zero, is not. This apparent anomaly is attributed to a random noise (that would require a markedly high amount of additional computation hours to be mitigated) stemming from a still incomplete sampling of the parameters space (despite our analysis incorporates an extensive number of random samples). We then identify a threshold value, i.e., $B = 0.17$ (average value observed in correspondence of instances associated with a value for B that should otherwise be expected to vanish), as a benchmark for evaluating the adequacy of parameter sampling within our sensitivity analysis. Consequently, we disregard from our sensitivity analysis instances in which B falls below 0.17 to enhance interpretability of visual representations of B, ST, $AMAV$, and $AMAE$.

Overall, the evaporation rate at Bruche is primarily influenced by the properties of the litter layer and the canopy (see Fig. 8). The litter

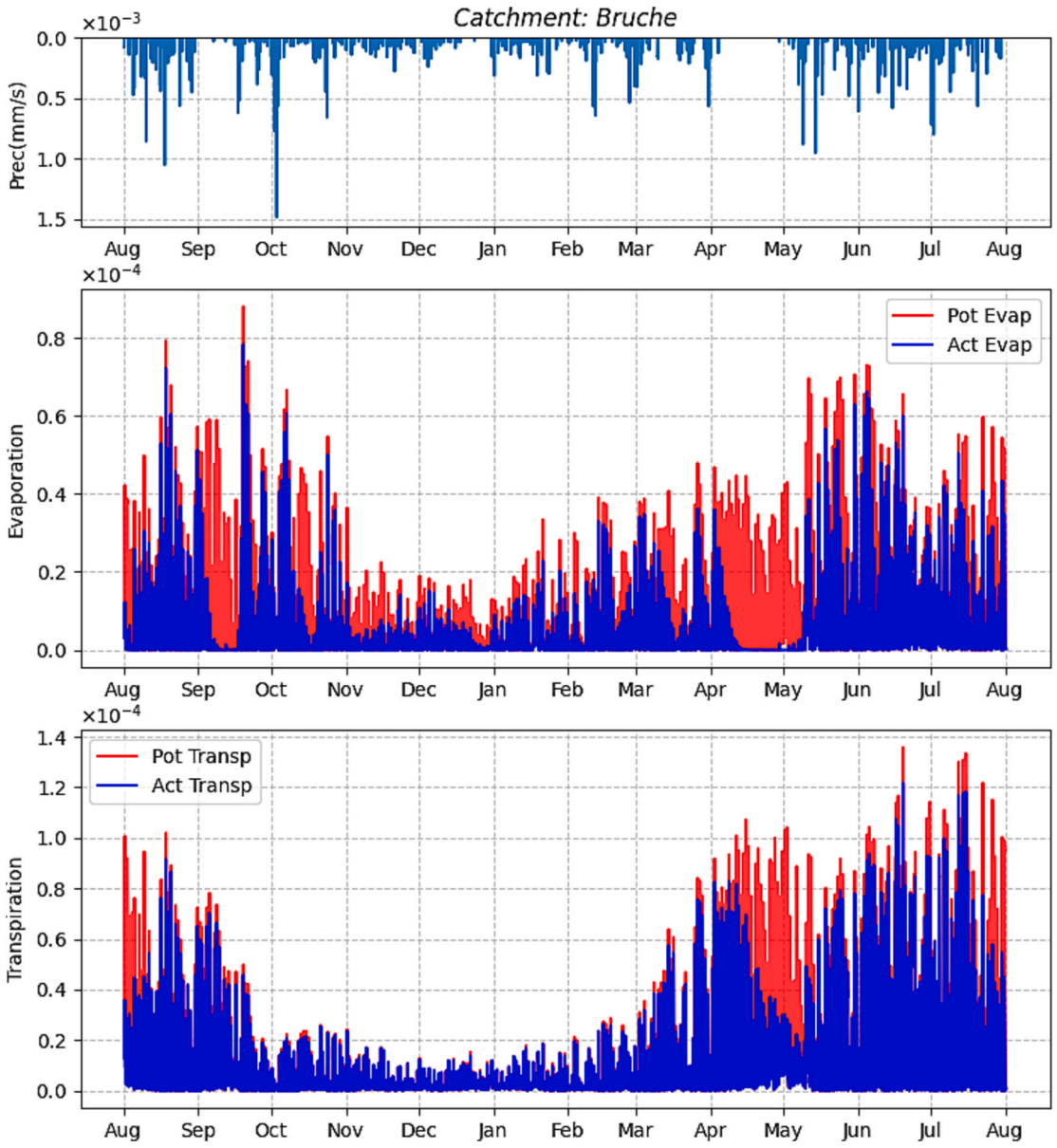

Fig. 5. Precipitation (top), potential (red) and actual (blue) evaporation and transpiration fluxes at the pixel located in the Bruche catchment. (For interpretation of the references to color in this figure legend, the reader is referred to the web version of this article.)

drainage coefficient significantly affects the evaporation rate throughout most of the year, exhibiting similar sensitivity patterns in terms of *B*, *ST*, *AMAV*, and *AMAE*. Notably, the *B* values associated with the litter drainage coefficient are less pronounced than those linked to other key parameters, such as the canopy radiation attenuation coefficient. This suggests that variations in the litter drainage coefficient primarily impact the variance and expected value of the evaporation rate at Bruche (as reflected in *ST*, *AMAV*, and *AMAE*), while having a lower influence on other statistical features of the pdf (e.g., skewness and kurtosis). During the fall and winter period (October to late March; see Fig. 3a), relatively high *ST*, *AMAV*, and *AMAE* values for the litter drainage coefficient are observed, coinciding with generally low evaporation rates (see Fig. 3b). Analysis of rainfall events during this period indicates that these elevated sensitivity values typically occur during soil-drying phases following relatively mild rain events (e.g., early November, late December, or the first half of March). This trend reflects water-limited evaporation dynamics, consistent with the observed low or declining evaporation rates during these drying intervals. In contrast, the sensitivity of the evaporation rate to litter layer thickness exhibits more intermittent patterns throughout the year. Interestingly, the diverse sensitivity indices (*B*, *ST*, *AMAV*, and *AMAE*) for litter layer thickness display similar magnitudes, indicating that this parameter impacts various statistical features of the evaporation pdf to a comparable extent. Regarding canopy properties, the radiation attenuation coefficient demonstrates high sensitivity across all sensitivity indices during the wet-soil and vegetative period (late May to early September), a time characterized by more frequent rain events and generally higher evaporation rates (see Fig. 3a-b). These observations align with the earlier discussion indicating that actual transpiration at Bruche is predominantly energy-limited during the wet and vegetative seasons, driven by the availability of solar radiation reaching the soil. During the drier fall and winter periods, we observe alternating sensitivity patterns (across all indices) to (*i*) the canopy radiation attenuation coefficient and (*ii*) the litter layer drainage coefficient. Under generally dry-soil conditions, water evaporation increases during or immediately after a rain event, with the rate being primarily energy-limited. As the soil becomes drier, evaporation decreases and transitions to a water-limited regime. Notably, the *AMAV* and *AMAE* indices for the canopy radiation

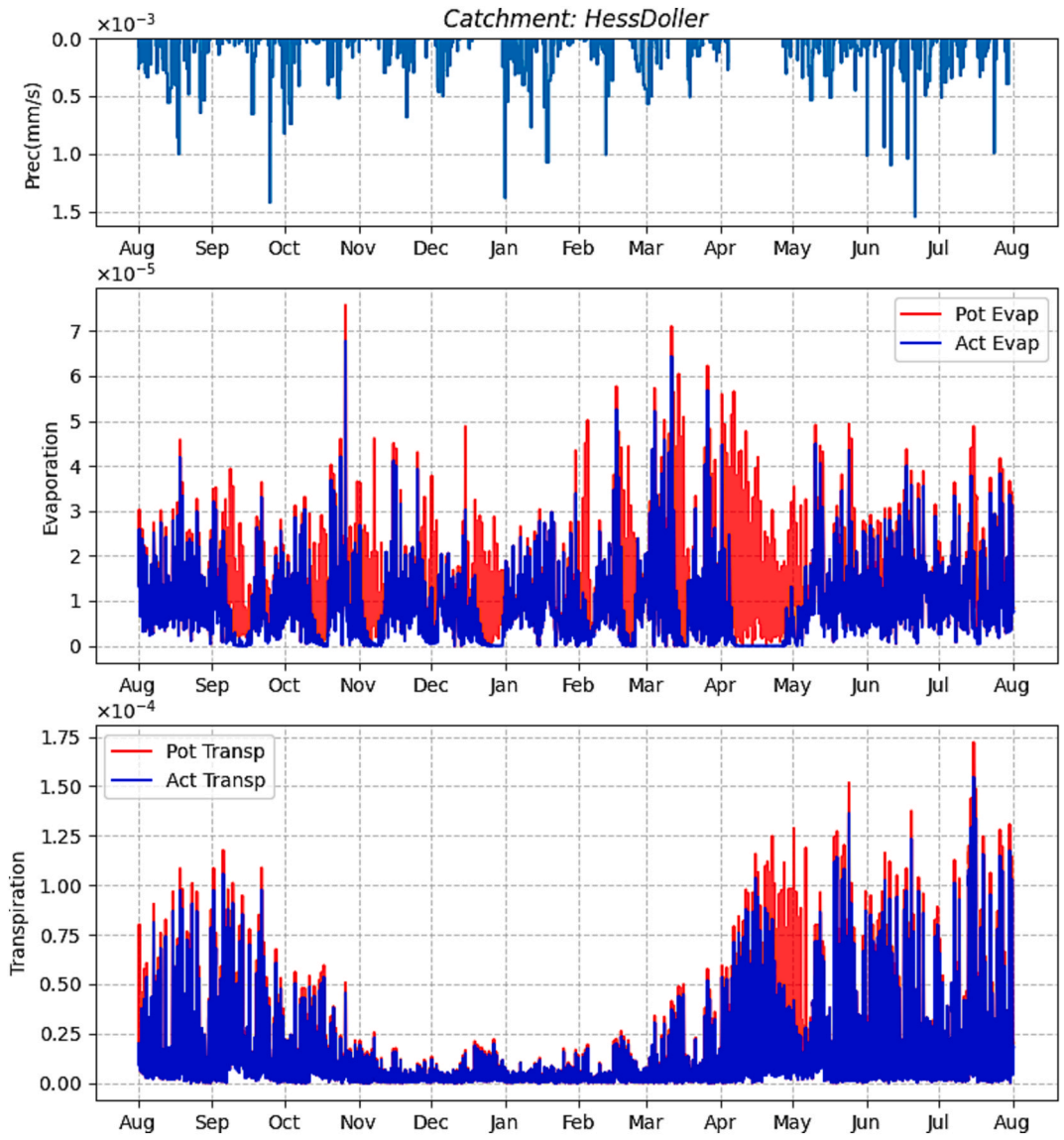

Fig. 6. Precipitation (top), potential (red) and actual (blue) evaporation and transpiration fluxes at the pixel located in the Doller catchment. (For interpretation of the references to color in this figure legend, the reader is referred to the web version of this article.)

attenuation coefficient are generally higher than the corresponding *B* and *ST* values during the drier months. This indicates that the canopy radiation attenuation coefficient exerts a strong influence on the variability of the first two statistical moments of the evaporation rate. Additionally, *AMAV* and *AMAE* values for canopy height are highest during the fall and winter and exhibit patterns similar to those associated with the canopy radiation attenuation coefficient. Since canopy height modulates the overall impedance to both water and energy fluxes, the observed similarity in *AMAV* and *AMAE* patterns for canopy height and the radiation attenuation coefficient (an energy-related parameter) suggests that, during the dry fall and winter periods, canopy height primarily influences the amount of energy reaching the soil, thereby regulating energy availability for transpiration. A similar observation holds for the trends of *B* and *ST* for the canopy height and radiation attenuation coefficient during the wet spring/summer period.

Considering evaporation at Doller (see Fig. 9), during the fall-winter period, we observe similar alternating sensitivity patterns to those documented at Bruche. Specifically, (*i*) the litter layer drainage coefficient exhibits high sensitivity following rain events, when the soil is drying and evaporation rates are declining, and (*ii*) the canopy radiation attenuation coefficient for vegetation type T2 shows higher sensitivity values during or at the end of rain events. However, the sensitivity to the canopy radiation attenuation coefficient is less pronounced at Doller compared to Bruche. Additionally, the sensitivity (across all indices) of evaporation to the canopy radiation attenuation coefficient for vegetation type T3 is less significant. On the other hand, indices *B*, *ST*, and *AMAV* for the canopy height of vegetation T2 show high values during the wet-soil period of late spring and summer, when the evaporation rate fluctuates around an approximately constant average value (see Fig. 4b). In contrast, *AMAE* remains generally low during this period. This suggests that the canopy height of vegetation T2, likely through its regulation of energy flux impedance toward the soil, primarily controls the uncertainty (around a stable mean) in evaporation rates during energy-limited periods with wet soil. During the fall and winter, indices *B*, *ST*, and *AMAV* for the canopy height of vegetation T2 generally exhibit higher values in correspondence with mid-to-high evaporation rates (e.g., late October, late November, and throughout February; see Fig. 9). This occurs when the soil remains wet, and water evaporation is governed by the amount of energy passing through the canopy (see potential and actual evaporation in Fig. 6). A similar trend is observed for the canopy height of vegetation type T3, indicating a combined influence of canopy height on energy-limited evaporation during the fall-winter

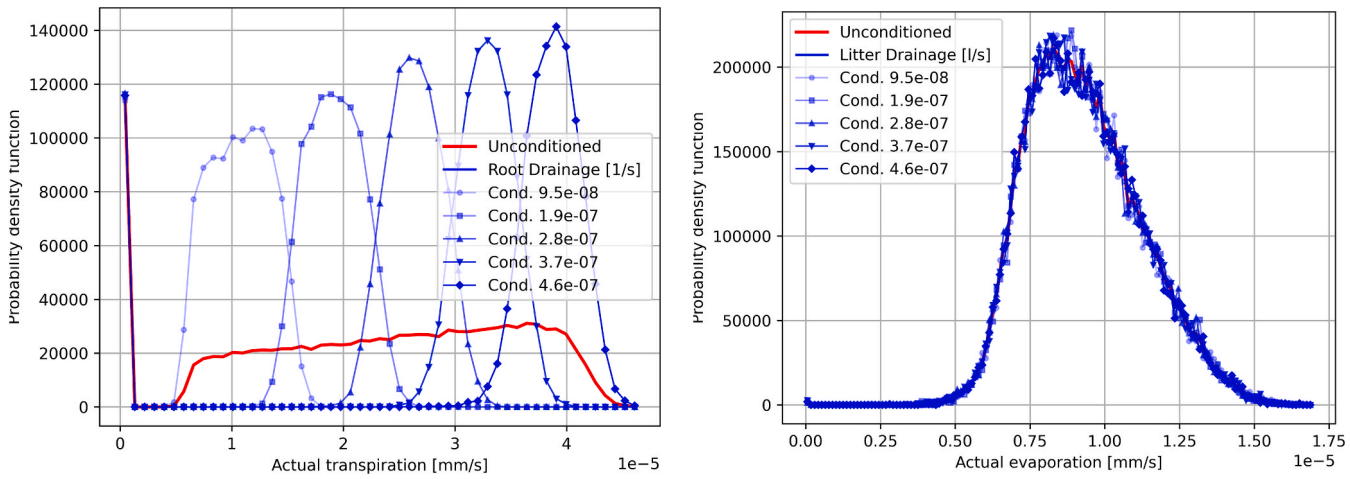

Fig. 7. Probability density functions related to: (a) transpiration on June 15th 2007 at 12 a.m. at Bruche with prescribed root drainage rate; (b) transpiration on October 6th 2006 at 1.p.m. at Doller with prescribed litter drainage rate. In each panel, we consider the unconditional (red curve) pdf of each output and its counterparts conditioned (blue curves) on five different (equally probable) subintervals (middle bin conditioning value, denoted as Cond., is provided in the legend) according to which the support of a given parameter is partitioned. (For interpretation of the references to color in this figure legend, the reader is referred to the web version of this article.)

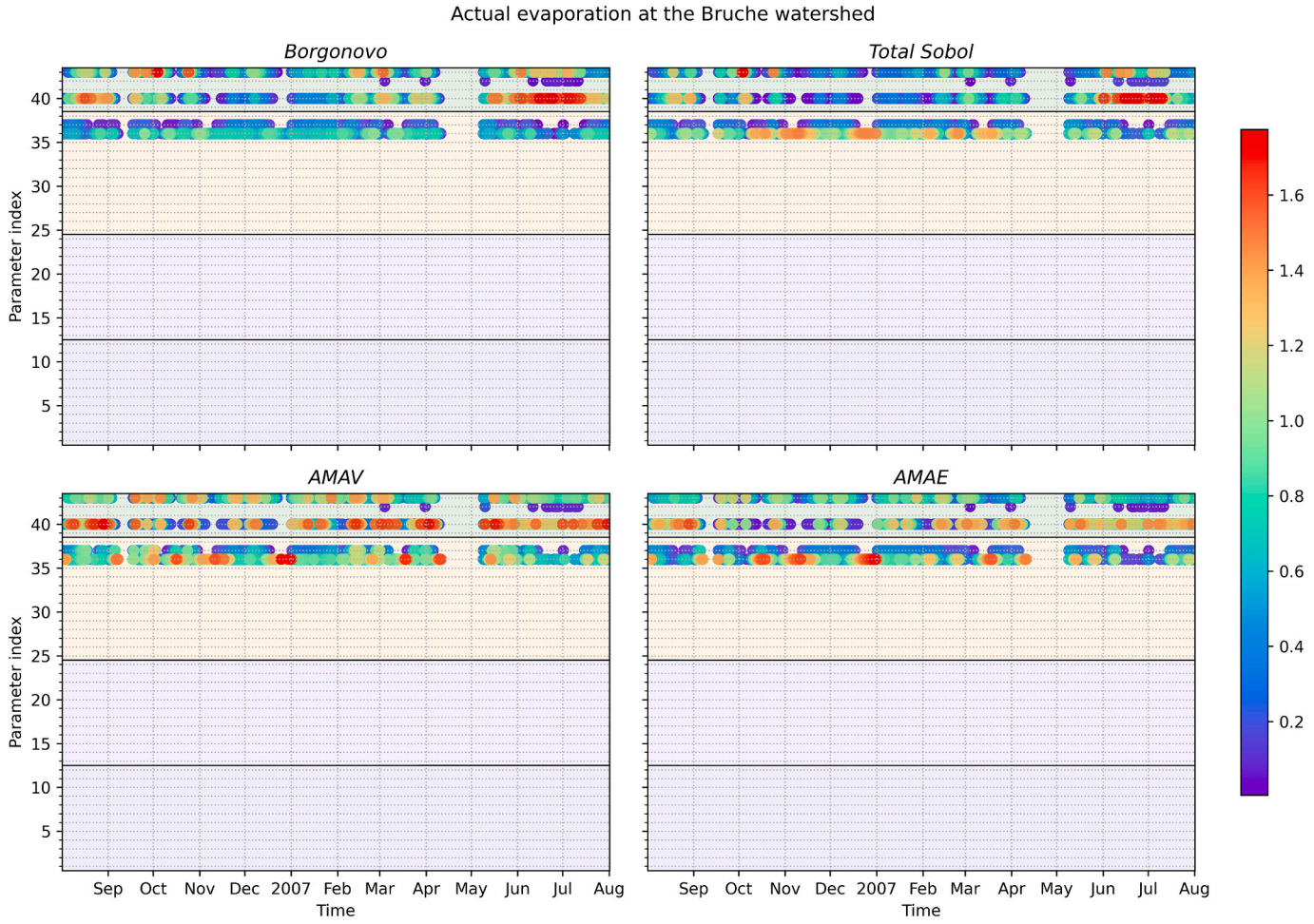

Fig. 8. Temporal behavior of the sensitivity indices related to the evaporation rate at the Bruche catchment. Parameter id = 36 denotes litter layer drainage rate, 37 litter layer thickness, 40 canopy radiation attenuation coefficient, 43 canopy height (see Supplementary Material for the complete list of parameter identifiers).

period at Doller.

Considering transpiration at Bruche (see Fig. 10), the litter layer drainage rate significantly influences the variability of the first (*AMAE*) and second (*AMAV*) statistical moments during periods of overall low transpiration, such as the generally dry-soil conditions in fall and winter. Since transpiration occurs exclusively within the root layer, this

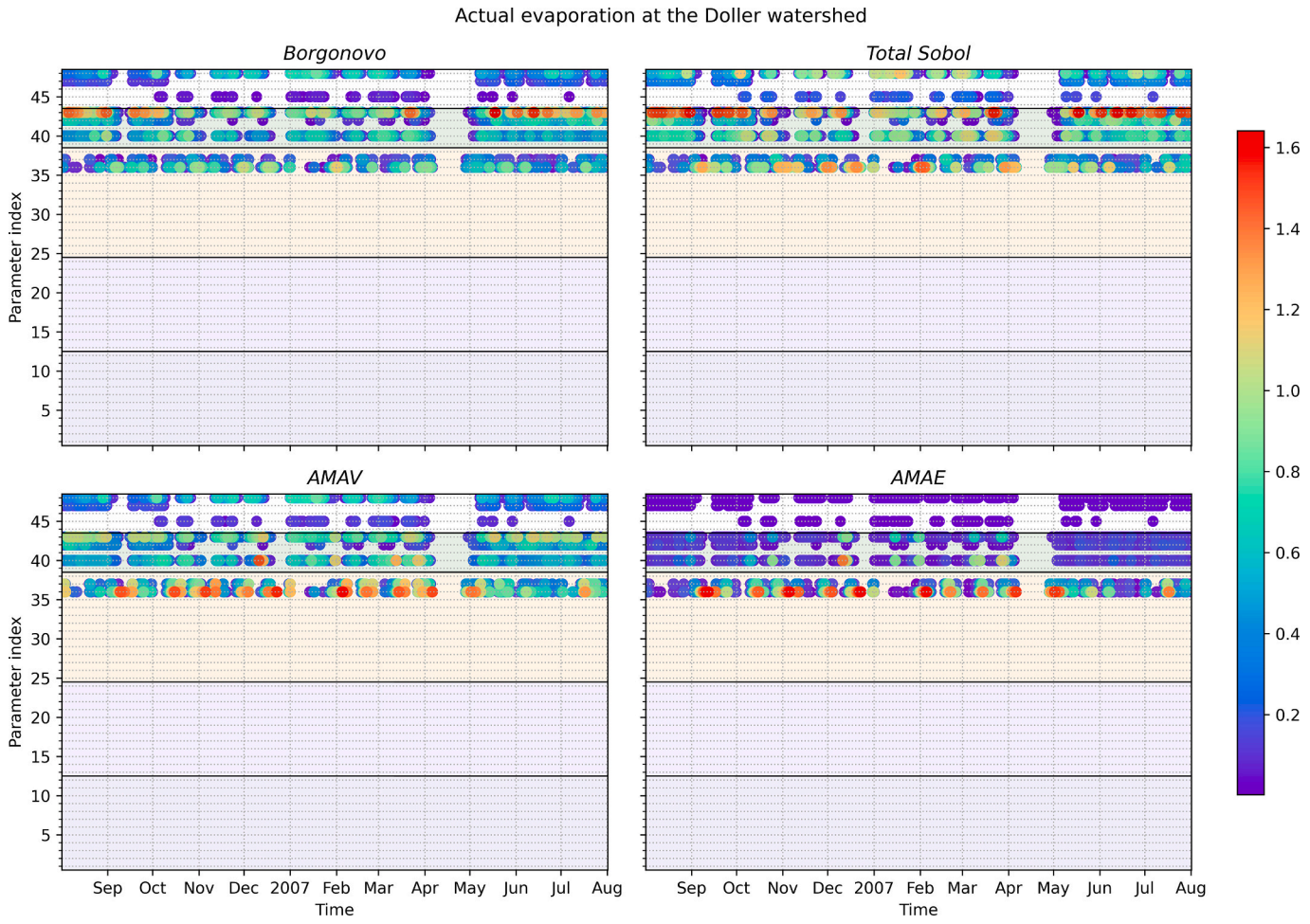

Fig. 9. Temporal behavior of the sensitivity indices related to evaporation at the Doller catchment. Parameter id = 36 denotes litter layer drainage rate, 37 litter layer thickness, for vegetation T2 40 canopy radiation attenuation coefficient, 42 maximum conductance of fully open stomata, 43 canopy height, and the counterparts for vegetation type T3 are 45, 47 and 48 (see Supplementary Material for the complete list of parameter identifiers).

sensitivity to the litter layer drainage rate likely reflects its role in regulating water availability as it percolates from the litter layer into the deeper root layers. Meanwhile, the corresponding *B* and *ST* values remain generally low during this period. During the late spring, summer, and early fall period, when precipitation is more frequent and the soil remains wetter, indices *B*, *ST*, *AMAV*, and even *AMAE* for the canopy radiation attenuation coefficient reach high values, particularly in the middle of summer. This observation indicates that the canopy's attenuation of radiation reaching the soil establishes energy-controlled dynamics for transpiration within the root layer under wet-soil conditions and high transpiration rates. Similarly, intense values of *B*, *ST*, *AMAV* for the canopy radiation attenuation coefficient are observed from February to March, when the soil at Bruche is generally dry, and transpiration begins to increase with the onset of the vegetative season (see Fig. 3c). This finding suggests that the canopy radiation attenuation coefficient plays a key role in controlling uncertainty in transpiration by influencing the variability in the energy available within the canopy (and, consequently, potential transpiration). Additionally, we note consistent sensitivity (across all indices and throughout the year) to the maximum conductance of fully open stomata, although the sensitivity values are not particularly pronounced. This suggests a partial but persistent control exerted by stomatal resistance on the water flux from leaves to the atmosphere, influencing transpiration dynamics. Moreover, during the very dry period in April (see Fig. 3a), there is notable sensitivity (across all indices) to the root layer drainage rate. This observation is consistent with the earlier discussion in Fig. 5, emphasizing the role of water availability in regulating transpiration under extremely dry soil conditions.

Regarding transpiration at Doller (see Fig. 11), there is significant sensitivity, as indicated by all uncertainty-related indices (*B*, *ST*, *AMAV*), to the maximum conductance of fully open stomata of vegetation T2 during the late spring and summer period. However, *AMAE* for this parameter remains relatively low during this time. A similar, albeit less marked, trend is observed for the canopy height of vegetation T2, with lower sensitivity values for *B*, *ST*, and *AMAV*.

Under the generally wet-soil conditions of late spring and summer, the expected value of transpiration remains approximately constant while there is a non-negligible uncertainty in the transpiration rates (see Fig. 4c). During this period, uncertainty in the maximum conductance of fully open stomata of vegetation T2 (and to a lesser extent that in the canopy height) drives uncertainty in transpiration rates. These results suggest that the maximum conductance of fully open stomata and the canopy height (influences the amount of energy available within the canopy) of vegetation T2 jointly regulate the overall resistance/impedance and energy availability for transpiration during the wet-soil spring/summer period, when water availability is not the primary limiting factor at Doller (see potential and actual transpiration in Fig. 6). Considering the fall and winter period, there is a balance in the sensitivity (particularly in terms of *B*, *AMAV*, and *ST*) to the maximum conductance of fully open stomata and to the canopy radiation attenuation coefficient of vegetation T2. Additionally, there is an increase in sensitivity to the albedo and *LAI* indices. These findings suggest a

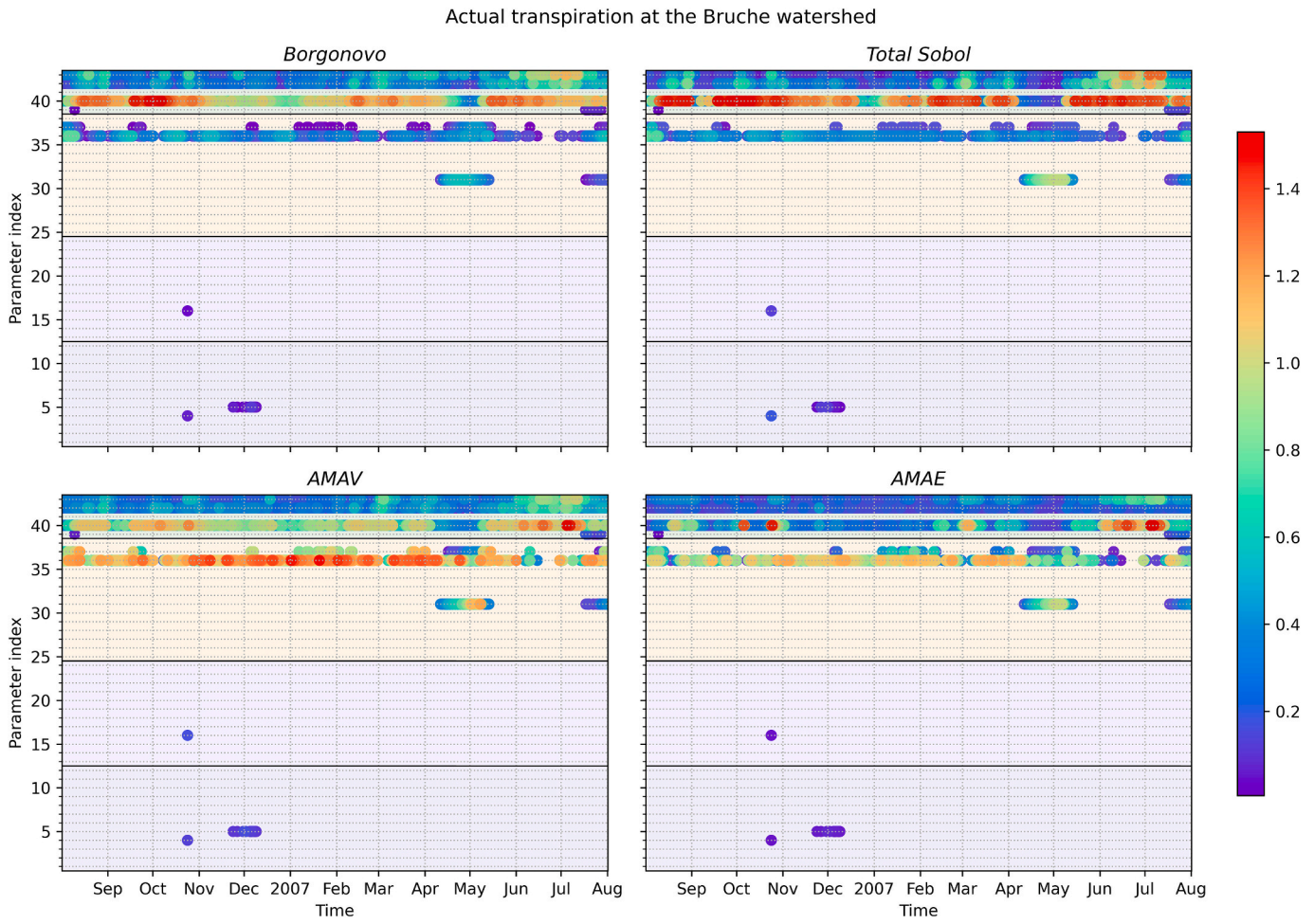

Fig. 10. Temporal behavior of the sensitivity indices related to transpiration at the Bruche catchment. Parameter id = 31 root layer drainage rate, 36 litter layer drainage rate, 37 litter layer thickness, 40 canopy radiation attenuation coefficient, 42 maximum conductance of fully open stomata, 43 canopy height (see Supplementary Material for the complete list of parameter identifiers).

combined control of stomatal resistance and energy availability on the uncertainty in transpiration rates during the fall-winter period. At the same time, lower sensitivity is observed with respect to properties of vegetation type T3.

Considering groundwater recharge at Bruche (see Fig. 12), there is a consistent sensitivity to the root layer drainage coefficient across all indices. In particular, high sensitivity values (for *B*, *ST*, and *AMAV*) are observed during and immediately after the very dry period of April, mirroring the sensitivity trends documented for transpiration. These results suggest a competition between transpiration and groundwater recharge for the limited water available in the root layer, with the root layer drainage coefficient playing a significant role in influencing both uncertainty (*B*, *ST*, *AMAV*) and average values (*AMAE*) of these water fluxes. Additionally, during the intense rain event at the beginning of October, when vegetation is mostly quiescent, the root layer drainage coefficient strongly impacts the groundwater recharge in terms of *B* and, to a lesser extent, *ST* and *AMAV*. This indicates that, in the absence of competition for water in the root layer, the uncertainty in the root layer drainage coefficient (which regulates the rate of water transfer to the underlying groundwater) chiefly affects higher-order statistical moments (e.g., peak and tail behavior) of the groundwater recharge pdf. Persistent sensitivity to the litter layer drainage coefficient, and to a lesser extent its thickness, is also observed during the drier fall and winter periods. This suggests that evaporation dynamics exert a significant influence on subsequent groundwater recharge under dry soil conditions and during vegetation dormancy (see Fig. 3a-c). In the summer period, sensitivity to vegetation-related parameters such as the rainfall interception coefficient, canopy radiation attenuation coefficient, and canopy height is evident across all indices. These findings imply that the rainfall interception coefficient impacts the amount of water reaching the root layer, while the canopy radiation attenuation coefficient and canopy height influence the water left as groundwater recharge in the root layer after plant transpiration.

With regard to groundwater recharge at Doller (see Fig. 13), there is persistent sensitivity to the root layer drainage coefficient throughout the year, as well as to the root layer height of vegetation T2 during the fall and winter period. Notably, during the fall/winter season, all sensitivity indices for the root layer drainage coefficient (and to a lesser extent for the root layer height of vegetation T2) show heightened values in correspondence with rain events (see Fig. 4a, d). This highlights the control exerted by the root layer drainage coefficient on water transfer to the groundwater, particularly in the absence of competition with transpiration. During and immediately after the very dry period in April, the root layer drainage coefficient shows high sensitivity only in terms of *AMAE*. This suggests that during periods of intense competition with plant transpiration at Doller, the root layer drainage coefficient predominantly influences the expected value of groundwater recharge, with a reduced impact on its uncertainty. During the generally wet-soil spring and summer period, sensitivity across all indices is observed for groundwater recharge with respect to the rainfall interception coefficient and the maximum conductance of fully open stomata of vegetation type T2. This indicates a dual control mechanism: the rainfall

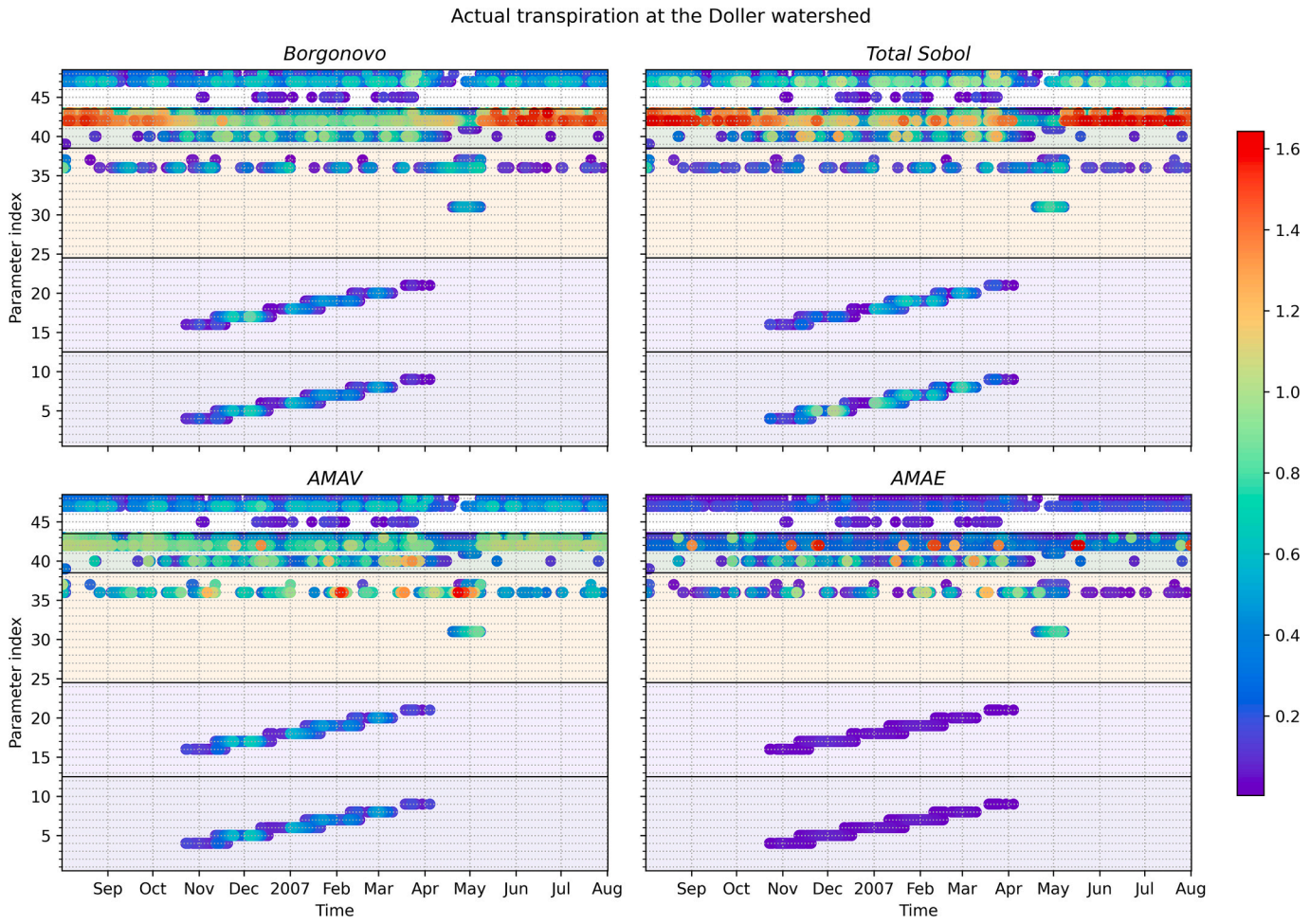

Fig. 11. Temporal behavior of the sensitivity indices related to transpiration at the Doller catchment. Parameter id from 1 to 12 correspond to *LAI*; parameter id from 13 to 24 correspond to albedo. Parameter 31 corresponds to root layer drainage rate, 36 to litter layer drainage rate and 37 to litter layer thickness. Parameter 40 (resp. 45) corresponds to the canopy radiation attenuation coefficient, 42 (resp. 47) to the maximum conductance of fully open stomata, 43 (resp. 48) to the canopy height for the vegetation type T2 (resp. vegetation type T3), (see Supplementary Material for the complete list of parameter identifiers).

interception coefficient affects the amount of water reaching the soil, while the maximum conductance of fully open stomata determines the portion of water not lost to plant transpiration. Conversely, no meaningful sensitivity is detected for the parameters associated with vegetation type T3.

5. Discussion

To summarize the key results of the sensitivity analysis performed for evaporation, transpiration, and groundwater recharge rates, Table 6 lists the key sensitive parameters (identified by a '✓' symbol) for each model output.

Evaporation only takes place in the top litter layer and is directly related to the energy flow through the canopy that then reaches ground surface where the litter layer drainage coefficient regulates the water drainage. As one could expect, transpiration appears as mainly influenced by the vegetation characteristics, while *LAI* and albedo coefficients impose an energy-constrain during the wet-soil winter period at Doller. Surprisingly, groundwater recharge is not sensible to any vegetation parameters, except the root layer thickness at Doller during fall/winter and the rainfall intercept at both catchments during Summer (at Doller also the maximum stomatal conductance plays a nonnegligible role). This is possibly related to the observation that groundwater recharge appears only when precipitations are significant and/or when transpiration rates are very small due to a reduced energy (for example during winter). When transpiration is significant, recharge to groundwater takes place solely after a period of precipitations that allows transpiration and replenishment of the water stored in the unsaturated zone.

Our results can be also viewed from a water- and energy-limitation perspective and according to the documented seasonal hydrological regime. During water-limited periods (e.g., winter at Bruche) evaporation is low and strongly influenced by the litter drainage coefficient, which modulates availability of water in the litter layer where evaporation takes place. In contrast, during wetter periods, evaporation becomes energy-limited, and sensitivity shifts toward vegetation-related parameters, such as the radiation attenuation coefficient. A similar pattern is observed for transpiration. During dry conditions, the hydraulic behavior of the litter layer plays a central role in regulating water availability in the root zone, where transpiration draws moisture. Transpiration becomes primarily energy-limited under wet conditions (e.g., summer at Doller), and vegetation-related parameters (e.g., canopy radiation attenuation coefficient, maximum stomatal conductance) gain importance as they modulate energy availability. With reference to groundwater recharge, dry periods are characterized by competition for water in the root zone between recharge and transpiration (assuming no energy limitation). In these cases, hydraulic properties of the root zone become critical, as they influence root uptake and percolation to deeper layers. When transpiration is low, these hydraulic properties primarily control the percolation process. During wet periods, competition

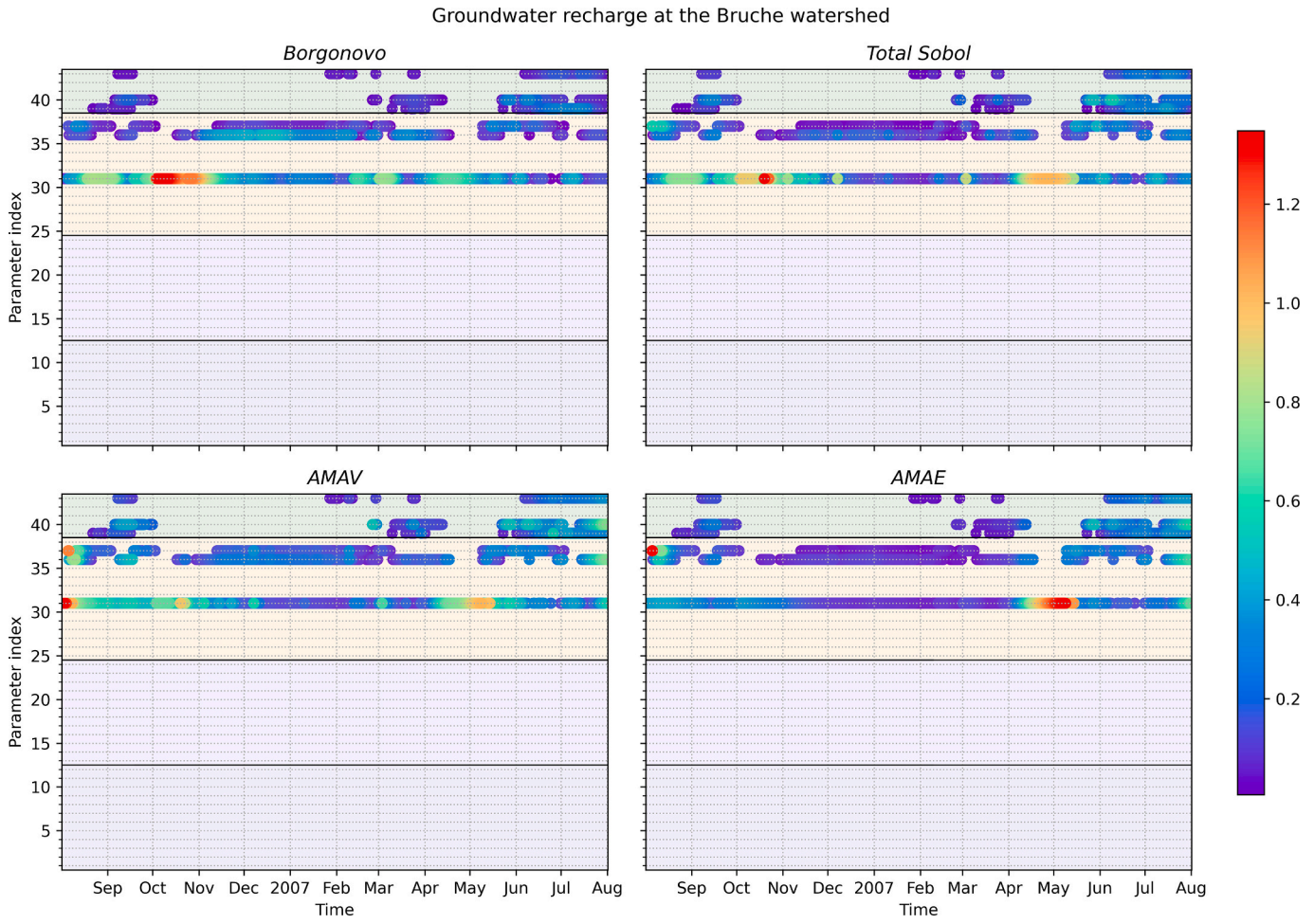

Fig. 12. Temporal behavior of the sensitivity indices related to groundwater recharge at the Bruche catchment. Parameter id = 31 root layer drainage rate, 36 litter layer drainage rate, 37 litter layer thickness, 39 rainfall interception coefficient, 40 canopy radiation attenuation coefficient, 43 canopy height (see Supplementary Material for the complete list of parameter identifiers).

between transpiration and recharge is again sensitive to vegetation parameters, which regulate the energy available for transpiration and thus indirectly affect water partitioning in the root zone.

Our results demonstrate the interest and potential of ab initio sensitivity analyses. We suggest that these types of studies should always be performed prior to running (either in a forward or in a stochastic inverse modeling context) a (land surface) model. Doing so enables one to:

- identify parameters and processes that require special attention due to their impact on target model results;
- obtain a quantitative appraisal of the importance of new features/processes that can eventually arise when considering development of various levels of complexity for a given model formulation;
- guide (stochastic) model calibration (see e.g., Ciriello et al., 2015, Guse et al., 2020, Dell'Oca et al., 2023a, Larabi et al., 2023) considering that uninfluential parameters cannot be reliably estimated and an a priori value can be acceptable (we recall here that a parameter can be sensitive while not being identifiable, e.g., because of its strong correlation to other parameters).

Results of a (global or local) sensitivity analysis are typically model- and site- (in terms of, e.g., climatic conditions, type of soils cover, type of soil, depending on the scale of the pixel) dependent. Even when diverse LSMs share some parameters, the relative importance of these parameters may vary, requiring ad hoc analyses, for which the illustrated methodological framework provides a viable approach. This is consistent with the observation that sensitivity analysis outcomes can be influenced by the degree of uncertainty in model parameters, typically reflected by their assumed variability ranges. As our knowledge of the system improves (through calibration efforts or assimilation/integration of new data) these uncertainty ranges may change. In turn, results of a sensitivity analysis should be revisited to capture any shifts in parameter relevance (e.g., Paleari and Confalonieri, 2016; Shin et al., 2013; Wang et al., 2013; Kelleher et al., 2013; Dell'Oca et al., 2020).

Furthermore, it is important to note that the formulation and assumptions underlying a given LSM are designed to reflect the hydrological, vegetative and energy conditions of the catchments under investigation. Thus, caution is needed when transferring results and conclusions drawn on the basis of our multi-method sensitivity analysis to other catchments. Different catchments might require alternative LSM structures and assumptions to capture local dynamics. We recall that each LSM implements various degrees of complexities for diverse processes. It is also recognized that uncertainty sources affecting land surface models typically comprise incomplete knowledge in (*a*) conceptual and mathematical formulation of models and processes therein and (*b*) parameters embedded in such models. As such, future research efforts will be focused at extending our knowledge on the quantification of the relative impact of uncertain processes (in terms of their mathematical formulation and parameterization; see e.g., Dell'Oca et al., 2020) on the diverse components of the water budget included in a land surface model.

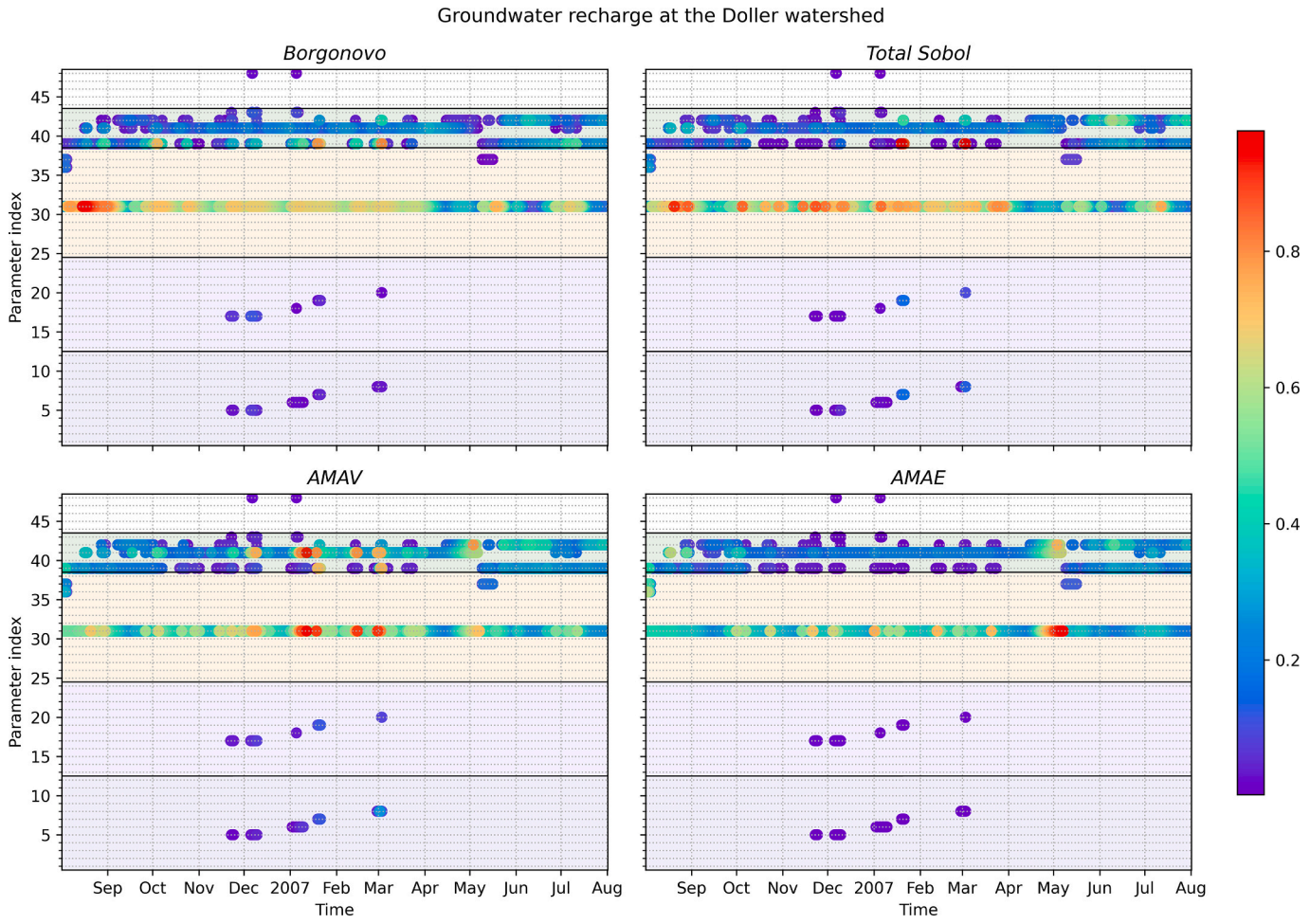

Fig. 13. Temporal behavior of the sensitivity indices related to groundwater recharge at the Doller catchment. Parameter id 31 corresponds to the root layer drainage rate. Parameters 39 corresponds to the rainfall interception coefficient, 41 to the root layer thickness and 42 to the maximum conductance of fully open stomata for vegetation type T2 (see Supplementary Material for the complete list of parameter identifiers).

6. Conclusions

We focus on the diagnosis of the behaviour of the recently developed NIHM (Normally Integrated Hydrological Model) modular Land Surface model. The latter embeds a variety of critical hydrological processes. Similar to other land surface models, it is characterized by a marked degree of parametrization. Temporal dynamics of water fluxes associated with transpiration, evaporation, and groundwater recharge are analyzed through global sensitivity analysis to discriminate relative importance of uncertain model parameters. Uncertainty sources comprise incomplete knowledge of monthly values of albedo and leaf area index, as well as of parameters related to vegetation and soil types constituting the litter layer and root zone. As opposed to previous studies on sensitivity analyses of land surface models, we provide an assessment of various aspects of sensitivity upon considering a joint analysis of multiple GSA metrics. These enable us to quantify the relative importance of our knowledge of a given model parameter on sensitivity metrics associated with the whole probability density function (pdf) (Eq. (4) of the target model outputs or its first two statistical moments (i.e., mean and variance; Eqs. (6), 7, and 8). Our analyses are exemplified through the simulation of realistic field settings characterizing two watersheds in the Vosges region (France) across a one-year period. In this sense, our study is anchored on field conditions (in terms of, e.g., climate, vegetation, and soil type) associated with these two watersheds. As the contribution of runoff to water balance in these two catchments is documented to be negligible, we do not include this process in our analyses.

Our study leads to the following major conclusions.

1. The strength of the relative importance of model parameters typically varies in time and depends on the statistical moment associated with the pdf of the model output of interest. For example, we document that the relative influence of the canopy height of vegetation T2 is generally higher for the variance than for the expected value of transpiration at Doller (Fig. 11). A similar observation holds considering the influence of the canopy radiation attenuation coefficient on transpiration at Bruche (Fig. 10).
2. Water fluxes related to evaporation at both catchments are chiefly influenced by the energy flow through the canopy and by the drainage in the top litter layer. Transpiration exhibits different behavior at Bruche and Doller. The litter drainage and the attenuation of radiation by the canopy constitute the major elements of influence at Bruche. Transpiration at Doller is mainly influenced by the latter quantity, albeit diverse vegetation-parameters (maximum conductance of fully open stomata, canopy height) are influential and also *LAI* and albedo (not evidenced at Bruche) display some degree of influence. Groundwater at both sites is majorly controlled by drainage in the root layer. At the same time, groundwater is sensitive (in a less marked fashion) to the litter properties at Bruche and to the vegetation properties at Doller. While most of these results can be intuitive, resting on rigorous GSA metrics yields an appropriate quantification of the relative strength of the way uncertainties

Table 6
Sensitivity of the target outputs of NIHM-LSM to uncertain input parameters. Key sensitive parameters are identified by a '✓' symbol.

Id	Parameter	Evaporation	Transpiration	Groundwater Recharge
1–12	Monthly *LAI*		✓	
13–24	Monthly Albedo		✓	
25	Radiation fraction for heat diffusion to the underground			
26	Sand fraction			
27	Clay fraction			
28	Root layer porosity			
29	Root layer field capacity			
30	Root layer residual water content			
31	Root layer drainage rate		✓	✓
33	Litter layer porosity			
34	Litter layer field capacity			
35	Litter layer residual water content			
36	Litter layer drainage rate	✓	✓	✓
37	Litter layer thickness	✓	✓	✓
39	Rainfall interception coefficient.			✓
40	Canopy radiation attenuation coefficient	✓	✓	✓
41	Root layer thickness			
42	Maximum conductance of fully open stomata	✓	✓	
43	Canopy height	✓	✓	✓

related to model parameters propagate onto different statistical moments of the pdf of the modeled water fluxes.

3. Relying on multiple sensitivity metrics, each focused on a given aspect of the uncertainty associated with a model response of interest, contributes to enhance our ability to quantify the relative importance of uncertainties linked to parameters of multiple origins. We note that a moment-independent analysis of the type linked to the distribution-based Borgonovo index may be subject to some operational constraints because of the need of assessing the complete pdf of the model output of interest. It can nevertheless be employed as a measure of the overall impact of a model parameter on the pdf of the water fluxes considered. When coupled with prior knowledge of the system functioning (as for example in the case where some processes or parameters are not involved in the computation of the water flux of interest), the results associated with this metric can be employed to gauge the quality of sampling of the model parameter space (see Section 3.2). The total Sobol indices and the *AMAV* indices provide very similar results in terms of ranking parameter importance with respect to water fluxes variance.

Future research will focus on improving our understanding of how uncertainties in process representation (in terms of mathematical formulation and parameterization (see, e.g., Dell'Oca et al., 2020)) affect the various components of the water budget in land surface models. In addition, we aim at integrating sensitivity analysis with stochastic calibration approaches to support efficient and informed LSM calibration (e.g., Dell'Oca et al., 2023b). This will also allow us to explore the way sensitivity results may vary depending on the level of uncertainty in model inputs, by comparing results obtained using a priori and post-calibration parameter distributions.

By demonstrating the operational value of multi-metric sensitivity analysis, our study offers a robust framework for guiding parameter selection and model refinement in water resource modeling under uncertainty.

CRediT authorship contribution statement

Aronne Dell'Oca: Writing – review & editing, Writing – original draft, Validation, Methodology, Conceptualization. **David Luttenauer:** Writing – original draft, Visualization, Software, Data curation. **Alberto Guadagnini:** Writing – review & editing, Writing – original draft, Methodology. **Sylvain Weill:** Writing – review & editing, Validation, Investigation. **Philippe Ackerer:** Writing – review & editing, Writing – original draft, Validation, Software, Methodology, Conceptualization.

Declaration of competing interest

The authors declare that they have no known competing financial interests or personal relationships that could have appeared to influence the work reported in this paper.

Acknowledgements

Daniel Luttenauer acknowledges support of the French Ministry of Agriculture and ENGEES for support through FCPR.

Alberto Guadagnini acknowledges the *Chaire Gutenberg* (Région Grand Est France, Strasbourg City and Strasbourg University).

Philippe Ackerer acknowledges support of the Politecnico di Milano (grant Senior Resident Researcher 2023).

Aronne Dell'Oca acknowledges support of the European Research Council (ERC) through the project HYPOR 101165321 and National Recovery and Resilience Plan (NRRP), Mission 4 Component 2 Investment 1.4 - Call for tender No. 3138 of December 16, 2021, rectified by Decree n.3175 of December 18, 2021 of Italian Ministry of University and Research funded by the European Union – NextGenerationEU; Project code CN_00000033, Concession Decree No. 1034 of June 17, 2022 adopted by the Italian Ministry of University and Research, CUP D43C22001250001, Project title "National Biodiversity Future Center - NBFC".

Appendix A. Supplementary data

Supplementary data to this article can be found online at https://doi.org/10.1016/j.jhydrol.2025.134310.

Data availability

The code and data will be made available using a shared folder upon request.

References

Baca Cabrera, J.C., 2021. The key role of stomatal conductance in controlling the grassland vegetation response to a changing environment (67. Technische Universität München.

Banque HYDRO. http://www.hydro.eaufrance.fr (last access: 4 February 2020).

Baroni, G., Tarantola, S., 2013. A general probabilistic framework for uncertainty and global sensitivity analysis of deterministic models: a hydrological case study. Environ. Model. Software 51, 26–34. https://doi.org/10.1016/j.envsoft.2013.09.022.

Bastidas, L.A., Hogue, T.S., Sorooshian, S., Gupta, H.V., Shuttleworth, W.J., 2006. Parameter sensitivity analysis for different complexity land surface models using multicriteria methods. J. Geophys. Res. Atmos. 111 (D20). https://doi.org/10.1029/2005JD006377.

Belfort, B., Toloni, I., Ackerer, P., Cote, S., Viville, D., Lehmann, F., 2018. Vadose Zone modeling in a small forested catchment: impact of water pressure head sampling frequency on 1D-model calibration. Geosciences 8, 72. https://doi.org/10.3390/geosciences8020072.

Beven, K.J., Smith, P.J., 2014. Concepts of information content and likelihood in parameter calibration for hydrological simulation models. J. Hydrol. Eng. https://doi.org/10.1061/(ASCE)HE.1943-5584.0000991.

Bianchi Janetti, E., Guadagnini, L., Riva, M., Guadagnini, A., 2019. Global sensitivity analyses of multiple conceptual models with uncertain parameters driving groundwater flow in a regional-scale sedimentary aquifer. J. Hydrol. 574, 544–556. https://doi.org/10.1016/j.jhydrol.2019.04.035.

Blyth, E.M., Arora, V.K., Clark, D.B., Dadson, S.J., De Kauwe, M.G., Lawrence, D.M., Melton, J.R., Pongratz, J., Turton, R.H., Yoshimura, K., Yuan, H., 2021. Advances in land surface modelling. Current Climate Change Reports 7, 45–71. https://doi.org/10.1007/s40641-021-00171-5.

Borgonovo, E., 2007. A new uncertainty importance measure. Reliab. Eng. Syst. Saf. 92, 771–784. https://doi.org/10.1016/j.ress.2006.04.015.

Boulet, G., Mougenot, B., Lhomme, J.-P., Fanise, P., Lili-Chabaane, Z., Olioso, A., Bahir, M., Rivalland, V., Jarlan, L., Merlin, O., Coudert, B., Er-Raki, S., Lagouarde, J.-P., 2015. The SPARSE model for the prediction of water stress and evapotranspiration components from thermal infrared data and its evaluation over irrigated and rainfed wheat. Hydrol. Earth Syst. Sci. 19, 4653–4672. https://doi.org/10.5194/hess-19-4653-2015.

Braud, I., Dantas-Antonino, A.C., Vauclin, M., Thony, J.L., Ruelle, P., 1995. A simple soil-plant-atmosphere transfer model (SiSPAT): development and field verification. J. Hydrol. 166, 213–250.

Brecciaroli, G., Cocco, S., Agnelli, A., Courchesne, F., Corti, G., 2012. From rainfall to throughfall in a maritime vineyard. Sci. Total Environ. 438, 174–188. https://doi.org/10.1016/j.scitotenv.2012.08.044.

Brewer, K., Clulow, A., Sibanda, M., Gokool, S., Odindi, J., Mutanga, O., Naiken, V., Chimonyo, V.G.P., Mabhaudhi, T., 2022. Estimation of maize foliar temperature and stomatal conductance as indicators of water stress based on optical and thermal imagery acquired using an unmanned aerial vehicle (UAV) platform. Drones 6, 169. https://doi.org/10.3390/drones6070169.

Campos, J., García-Ruíz, F., Gil, E., 2021. Assessment of vineyard canopy characteristics from vigour maps obtained using UAV and satellite imagery. Sensors 21, 2363. https://doi.org/10.3390/s21072363.

Carter, G.A., 1998. Reflectance wavebands and indices for remote estimation of photosynthesis and stomatal conductance in pine canopies. Remote Sens. Environ. 63, 61–72. https://doi.org/10.1016/S0034-4257(97)00110-7.

Ceresa, L., Guadagnini, A., Rodríguez-Escales, P., Riva, M., Sanchez-Vila, X., Porta, G.M., 2023. On multi-model assessment of complex degradation paths: the fate of diclofenac and its transformation products. Water Resour. Res. 59, e2022WR033183. https://doi.org/10.1029/2022WR033183.

Chambre Régionale d'Agriculture Grand Est, 2011. Base de données du Référentiel Régional Pédologique d'Alsace: carte des pédopaysages d'Alsace à 1/250 000, en format DoneSol IGCS.

Chambre Régionale d'Agriculture Grand Est, 2015. Base de données du Référentiel Régional Pédologique de Lorraine: carte des pédopaysages de Lorraine à 1/250 000, en format DoneSol IGCS.

Charreyron, M., 2011. Suivi de la transpiration et de la conductance stomatique chez le pommier sous trois régimes hydriques: irrigation, sécheresse et réhydratation. Université Blaise Pascal (Clermont Ferrand 2).

Choudhury, B.J., Monteith, J.L., 1988. A four-layer model for the heat budget of homogeneous land surfaces. Q. J. R. Meteorolog. Soc. 114, 373–398. https://doi.org/10.1002/qj.49711448006.

Ciriello, V., Edery, Y., Guadagnini, A., Berkowitz, B., 2015. Multimodel framework for characterization of transport in porous media. Water Resour. Res. 51, 3384–3402. https://doi.org/10.1002/2015WR017047.

Clapp, R.B., Hornberger, G.M., 1978. Empirical equations for some soil hydraulic properties. Water Resour. Res. 14, 601–604. https://doi.org/10.1029/WR014i004p00601.

Clothier, B.E., Clawson, K.L., Pinter, P.J., Moran, M.S., Reginato, R.J., Jackson, R.D., 1986. Estimation of soil heat flux from net radiation during the growth of alfalfa. Agric. For. Meteorol. 37, 319–329. https://doi.org/10.1016/0168-1923(86)90069-9.

Copernicus Climate Change Service. (2018). Leaf area index and fraction absorbed of photosynthetically active radiation 10-daily gridded data from 1981 to present. doi: 10.24381/CDS.7E59B01A.

Couturier, D.E., Ripley, E.A., 1973. Rainfall interception in mixed grass prairie. Can. J. Plant Sci. 53, 659–663. https://doi.org/10.4141/cjps73-130.

Cox, P.M., Huntingford, C., Harding, R.J., 1998. A canopy conductance and photosynthesis model for use in a GCM land surface scheme. J. Hydrol. 212–213, 79–94. https://doi.org/10.1016/S0022-1694(98)00203-0.

Dai, Y., Zeng, X., Dickinson, R.E., Baker, I., Bonan, G.B., Bosilovich, M.G., Yang, Z.L., 2003. The common land model. Bull. Am. Meteorol. Soc. 84 (8), 1013–1024. https://doi.org/10.1175/BAMS-84-8-1013.

Deardorff, J.W., 1978. Efficient prediction of ground surface temperature and moisture, with inclusion of a layer of vegetation. J. Geophys. Res. 83, 1889. https://doi.org/10.1029/JC083iC04p01889.

Decharme, B., Boone, A., Delire, C., Noilhan, J., 2011. Local evaluation of the interaction between soil biosphere atmosphere soil multilayer diffusion scheme using four pedotransfer functions. J. Geophys. Res. 116 (D20), D20126. https://doi.org/10.1029/2011JD016002.

Dell'Oca, A., 2023. Sensitivity analysis: an operational picture. Water Resour. Res. 59, e2022WR033780. https://doi.org/10.1029/2022WR033780.

Dell'Oca, A., Manzoni, A., Siena, M., Bona, N.G., Moghadasi, L., Miarelli, M., Renna, D., Guadagnini, A., 2023a. Stochastic inverse modeling of transient laboratory-scale three-dimensional two-phase core flooding scenarios. Int. J. Heat Mass Transf. 202, 123716.

Dell'Oca, A., Riva, M., Guadagnini, A., 2017. Moment-based metrics for global sensitivity analysis of hydrological systems. Hydrol. Earth Syst. Sci. 21, 6219–6234. https://doi.org/10.5194/hess-21-6219-2017.

Dell'Oca, A., Riva, M., Guadagnini, A., 2020. Global sensitivity analysis for multiple interpretive models with uncertain parameters. Water Resour. Res. 56, e2019WR025754. https://doi.org/10.1029/2019WR025754.

Dell'Oca, A., Guadagnini, A., Riva, M., 2023b. Probabilistic assessment of failure of infiltration structures under model and parametric uncertainty. J. Environ. Manage. 344, 118466. https://doi.org/10.1016/j.jenvman.2023.118466.

Demarty, J., Ottle, C., Braud, I., Olioso, A., Frangi, J.P., Gupta, H.V., Bastidas, L.A., 2005. Constraining a physically based soil-vegetation-atmosphere transfer model with surface water content and thermal infrared brightness temperature measurements using a multiobjective approach. Water Resour. Res. 41. https://doi.org/10.1029/2004WR003695.

Dingman, S.L., 2002. Physical hydrology, (2nd ed.). Prentice Hall.

Durand, Y., Brun, E., Merindol, L., Guyomarc'h, G., Lesaffre, B., Martin, E., 1993. A meteorological estimation of relevant parameters for snow models. Ann. Glaciol. 18, 65–71. https://doi.org/10.3189/S0260305500011277.

Durand, Y., Giraud, G., Laternser, M., Etchevers, P., Mérindol, L., Lesaffre, B., 2009. Reanalysis of 47 Years of climate in the French Alps (1958–2005): Climatology and Trends for Snow Cover. J. Appl. Meteorol. Climatol. 48, 2487–2512. https://doi.org/10.1175/2009JAMC1810.1.

Escamilla, J.A., Comerford, N.B., Neary, D.G., 1991. Soil-core break method to estimate pine root distribution. Soil Sci. Soc. Am. J. 55, 1722–1726. https://doi.org/10.2136/sssaj1991.03615995005500060036x.

European Union – SOeS, 2018. CORINE Land Cover.

Ferretti, F., Saltelli, A., Tarantola, S., 2016. Trends in sensitivity analysis practice in the last decade. Sci. Total Environ. 568, 666–670. https://doi.org/10.1016/j.scitotenv.2016.02.133.

Fisher, R.A., Koven, C.D., 2020. Perspectives on the future of land surface models and the challenges of representing complex terrestrial systems. J. Adv. Model. Earth Syst. 12, e2018MS001453. https://doi.org/10.1029/2018MS001453.

Freeling, M., Walbot, V., (Eds.). 1994. The Maize Handbook. Springer. doi: 10.1007/978-1-4612-2694-9.

Friesen, J., Van Stan, J.T., 2019. Early European observations of precipitation partitioning by vegetation: a synthesis and evaluation of 19th century findings. Geosciences 9, 423. https://doi.org/10.3390/geosciences9100423.

Gowdy, M., Pieri, P., Suter, B., Marguerit, E., Destrac-Irvine, A., Gambetta, G., van Leeuwen, C., 2022. Estimating bulk stomatal conductance in grapevine canopies. Front. Plant Sci. 13. https://doi.org/10.3389/fpls.2022.839378.

Grassland: Mission: Biomes. (n.d.). https://earthobservatory.nasa.gov/biome/biograssland.php (Ultimo accesso: 30 maggio 2023).

Guse, B., Pfannerstill, M., Fohrer, N., Gupta, H., 2020. Improving information extraction from simulated discharge using sensitivity-weighted performance criteria. Water Resour. Res. 56, e2019WR025605. https://doi.org/10.1029/2019WR025605.

Habets, F., Boone, A., Champeaux, J.L., Etchevers, P., Franchistéguy, L., Leblois, E., Ledoux, E., Le Moigne, P., Martin, E., Morel, S., Noilhan, J., Quintana Seguí, P., Rousset-Regimbeau, F., Viennot, P., 2008. The SAFRAN-ISBA-MODCOU hydrometeorological model applied over France. J. Geophys. Res. 113, D06113. https://doi.org/10.1029/2007JD008548.

Hogue, T.S., Bastidas, L.A., Gupta, H.V., Sorooshian, S., 2006. Evaluating model performance and parameter behavior for varying levels of land surface model complexity. Water Resour. Res. 42 (8). https://doi.org/10.1029/2005WR004440.

Hovenden, M.J., Brodribb, T., 2000. Altitude of origin influences stomatal conductance and therefore maximum assimilation rate in Southern Beech Nothofagus Cunninghamii. Funct. Plant Biol. 27, 451. https://doi.org/10.1071/PP99164.

IUSS Working Group WRB, 2022. World Reference Base for Soil Resources. International soil classification system for naming soils and creating legends for soil maps, (4th ed.). International Union of Soil Sciences (IUSS).

Jarvis, P.G., 1976. The Interpretation of the variations in leaf water potential and stomatal conductance found in canopies in the field. Philos. Trans. R. Soc., B 273, 593–610.

Jeannot, B., Weill, S., Eschbach, D., Schmitt, L., Delay, F., 2018. A Low-dimensional integrated subsurface hydrological model coupled with 2-D overland flow: application to a restored fluvial hydrosystem (Upper Rhine River – France). J. Hydrol. 563, 495–509. https://doi.org/10.1016/j.jhydrol.2018.06.028.

Jonard, F., André, F., Ponette, Q., Vincke, C., Jonard, M., 2011. Sap flux density and stomatal conductance of European beech and common oak trees in pure and mixed stands during the Summer drought of 2003. J. Hydrol. 409, 371–381. https://doi.org/10.1016/j.jhydrol.2011.08.032.

Ju, J., Dai, H., Wu, C., Hu, B., Ye, M., Chen, X., Gui, D., Liu, H., Zhang, J., 2021. Quantifying the uncertainty of the future hydrological impacts of climate change: comparative analysis of an advanced hierarchical sensitivity in humid and semiarid basins. J. Hydrometeorol. 22, 601–621. https://doi.org/10.1175/JHM-D-20-0016.1.

Kelleher, C., Wagener, T., McGlynn, B., Ward, A.S., Gooseff, M.N., Payn, R.A., 2013. Identifiability of transient storage model parameters along a mountain stream. Water Resour. Res. XX,. https://doi.org/10.1002/wrcr.20413.

Kergoat, L., 1998. A model for hydrological equilibrium of leaf area index on a global scale. J. Hydrol. 212–213, 268–286. https://doi.org/10.1016/S0022-1694(98)00211-X.

Kim, J., Verma, S.B., 1991. Modeling canopy stomatal conductance in a temperate grassland ecosystem. Agric. For. Meteorol. 55, 149–166. https://doi.org/10.1016/0168-1923(91)90028-O.
Kustas, W.P., Daughtry, C.S.T., 1990. Estimation of the soil heat flux/net radiation ratio from spectral data. Agric. For. Meteorol. 49, 205–223. https://doi.org/10.1016/0168-1923(90)90033-3.
Larabi, S., Mai, J., Schnorbus, M., Tolson, B.A., Zwiers, F., 2023. Towards reducing the high cost of parameter sensitivity analysis in hydrologic modeling: a regional parameter sensitivity analysis approach. Hydrol. Earth Syst. Sci. 27, 3241–3262. https://doi.org/10.5194/hess-27-3241-2023.
Lawrence, D.M., Fisher, R.A., Koven, C.D., Oleson, K.W., Swenson, S.C., Bonan, G., Zeng, X., 2019. The community land model version 5: description of new features, benchmarking, and impact of forcing uncertainty. J. Adv. Model. Earth Syst. 11 (12), 4245–4287. https://doi.org/10.1029/2018MS001583.
Leuschner, C., Hertel, D., Coners, H., Büttner, V., 2001. Root competition between beech and oak: a hypothesis. Oecologia 126, 276–284. https://doi.org/10.1007/s004420000507.
Li, J., Duan, Q.Y., Gong, W., Ye, A., Dai, Y., Miao, C., Di, Z., Tong, C., Sun, Y., 2013. Assessing parameter importance of the common land model based on qualitative and quantitative sensitivity analysis. Hydrol. Earth Syst. Sci. 17, 3279–3293. https://doi.org/10.5194/hess-17-3279-2013.
Liang, X., Guo, J., 2003. Intercomparison of land-surface parameterization schemes: sensitivity of surface energy and water fluxes to model parameters. J. Hydrol. 279 (1–4), 182–209. https://doi.org/10.1016/S0022-1694(03)00168-9.
Liu, J., Skidmore, A.K., Wang, T., Zhu, X., Premier, J., Heurich, M., Beudert, B., Jones, S., 2019. Variation of leaf angle distribution quantified by terrestrial LiDAR in natural European beech forest. ISPRS J. Photogramm. Remote Sens. 148, 208–220. https://doi.org/10.1016/j.isprsjprs.2019.01.005.
McCuen, R.H., 1973. The role of sensitivity analysis in hydrologic modeling. J. Hydrol. 18, 37–53. https://doi.org/10.1016/0022-1694(73)90024-3.
Mahhou, A., DeJong, T.M., Cao, T., Shackel, K.S., 2005. Water stress and crop load effects on vegetative and fruit growth of 'Elegant Lady' peach [Prunus persica (L.) batch] trees. Fruits 60, 55–68. https://doi.org/10.1051/fruits:2005013.
Mai, J., Craig, J.R., Tolson, B.A., Arsenault, R., 2022. The sensitivity of simulated streamflow to individual hydrologic processes across North America. Nat. Commun. 13 (1), 455. https://doi.org/10.1038/s41467-022-28010-7.
Maina, F.Z., Guadagnini, A., 2018. Uncertainty quantification and global sensitivity analysis of subsurface flow parameters to gravimetric variations during pumping tests in unconfined aquifers. Water Resour. Res. 54 (1), 501–518. https://doi.org/10.1002/2017WR021655.
Maina, F.Z., Siirila-Woodburn, E.R., 2020. The role of subsurface flow on evapotranspiration: a global sensitivity analysis. Water Resour. Res. 56, e2019WR026612. https://doi.org/10.1029/2019WR026612.
Maina, F.Z., Siirila-Woodburn, E.R., Dennedy-Frank, P.J., 2022. Assessing the impacts of hydrodynamic parameter uncertainties on simulated evapotranspiration in a mountainous watershed. J. Hydrol. 08, 127620. https://doi.org/10.1016/j.jhydrol.2022.127620.
Maneta, M.P., Silverman, N.L., 2013. A spatially distributed model to simulate water, energy, and vegetation dynamics using information from regional climate models. Earth Interact 17 (11), 1–44. https://doi.org/10.1175/2012EI000472.1.
Manabe, S., 1969. Climate and the ocean circulation. I. The atmospheric circulation and the hydrology of the earth's surface. Monthly Weather Review, 97(11), 739–774. doi: 10.1175/1520-0493(1969)097<0739:CATOC>2.3.CO;2.
Matese, A., Di Gennaro, S.F., Berton, A., 2017. Assessment of a canopy height model (CHM) in a vineyard using UAV-based multispectral imaging. Int. J. Remote Sens. 38, 2150–2160. https://doi.org/10.1080/01431161.2016.1226002.
Mueller, K.E., Tilman, D., Fornara, D.A., Hobbie, S.E., 2013. Root depth distribution and the diversity–productivity relationship in a long-term grassland experiment. Ecology 94, 787–793. https://doi.org/10.1890/12-1399.1.
Neitsch, S. L., Arnold, J. G., Kiniry, J. R., Williams, J. R., & King, K. W. (2002). Soil and Water Assessment Tool (SWAT) User's Manual, Version 2000. Grassland Soil and Water Research Laboratory, Blackland Research Center, Texas Agricultural Experiment Station, Texas Water Resources Institute.
Niu, G.-Y., Yang, Z.-L., Mitchell, K.E., Chen, F., Ek, M.B., Barlage, M., Kumar, A., Manning, K., Niyogi, D., Rosero, E., Tewari, M., Xia, Y., 2011. The Community noah land surface model with multiparameterization options (Noah-MP): 1. Model description and evaluation with local-scale measurements. J. Geophys. Res. Atmos. 116 (D12). https://doi.org/10.1029/2010JD015139.
Nicholas, K.A., Matthews, M.A., Lobell, D.B., Willits, N.H., Field, C.B., 2011. Effect of vineyard-scale climate variability on Pinot noir phenolic composition. Agric. For. Meteorol. 151, 1556–1567. https://doi.org/10.1016/j.agrformet.2011.06.010.
Ocheltree, T.W., Nippert, J.B., Prasad, P.V.V., 2012. Changes in stomatal conductance along grass blades reflect changes in leaf structure. Plant Cell Environ. 35, 1040–1049. https://doi.org/10.1111/j.1365-3040.2011.02470.x.
Overgaard, J., Rosbjerg, D., Butts, M.B., 2006. Land-surface modelling in hydrological perspective – a review. Biogeosciences 3, 229–241. https://doi.org/10.5194/bg-3-229-2006.
Paleari, L., Confalonieri, R., 2016. Sensitivity analysis of a sensitivity analysis: We are likely overlooking the impact of distributional assumptions. Ecological Modelling 340, 57–63.
Pan, Y., Weill, S., Ackerer, P., Delay, F., 2015. A coupled stream flow and depth-integrated subsurface flow model for catchment hydrology. J. Hydrol. 530, 66–78. https://doi.org/10.1016/j.jhydrol.2015.09.044.
Peel, M.C., Finlayson, B.L., McMahon, T.A., 2007. Updated world map of the Köppen-Geiger climate classification. Hydrol. Earth Syst. Sci. 11 (5), 1633–1644. https://doi.org/10.5194/hess-11-1633-2007.
Peiffer, J.A., Romay, M.C., Gore, M.A., Flint-Garcia, S.A., Zhang, Z., Millard, M.J., Gardner, C.A.C., McMullen, M.D., Holland, J.B., Bradbury, P.J., Buckler, E.S., 2014. The genetic architecture of maize height. Genetics 196, 1337–1356. https://doi.org/10.1534/genetics.113.159152.
Planque, C., 2018. Observation satellitaire et modélisation de l'albédo des forêts sur le territoire français métropolitain: dynamiques temporelles et impacts radiatifs (315 p.). Université Paul Sabatier - Toulouse III.
Quintana-Seguí, P., Le Moigne, P., Durand, Y., Martin, E., Habets, F., Baillon, M., Canellas, C., Franchisteguy, L., Morel, S., 2008. Analysis of near-surface atmospheric variables: validation of the SAFRAN analysis over France. J. Appl. Meteorol. Climatol. 47, 92–107. https://doi.org/10.1175/2007JAMC1636.1.
Razavi, S., Jakeman, A., Saltelli, A., Prieur, C., Iooss, B., Borgonovo, E., Plischke, E., Lo Piano, S., Iwanaga, T., Becker, W., Tarantola, S., Guillaume, J.H.A., Jakeman, J., Gupta, H., Melillo, N., Rabitti, G., Chabridon, V., Duan, Q., Sun, X., Smith, S., Sheikholeslami, R., Hosseini, N., Asadzadeh, M., Puy, A., Kucherenko, S., Maier, H. R., 2021. The future of sensitivity analysis: an essential discipline for systems modeling and policy support. Environ. Model. Software 137, 104954. https://doi.org/10.1016/j.envsoft.2020.104954.
Reis, M.G.D., Ribeiro, A., 2020. Conversion factors and general equations applied in agricultural and forest meteorology. Agrometeoros 27. https://doi.org/10.31062/agrom.v27i2.26527.
Richards, D., 2011. The Grape root System. In: Janick, J. (Ed.), Horticultural Reviews. John Wiley & Sons, pp. 127–168. https://doi.org/10.1002/9781118060728.ch3.
Saltelli, A., 2007. Sensitivity Analysis in Practice: a Guide to Assessing Scientific Models. Wiley.
Sandoval, L., Riva, M., Colombo, I., Guadagnini, A., 2022. Sensitivity analysis and quantification of the role of governing transport mechanisms and parameters in a gas flow model for low-permeability porous media. Transp. Porous Media 142 (3), 509–530. https://doi.org/10.1007/s11242-022-01755-x.
Saqr, A.M., Ibrahim, M.G., Fujii, M., Nasr, M., 2021. Sustainable Development Goals (SDGs) associated with groundwater over–exploitation vulnerability: Geographic information system–based multi–criteria decision analysis. Nat. Resour. Res. 30 (6), 4255–4276. https://doi.org/10.1007/s11053-021-09945-y.
Seibert, J., Vis, M.J.P., 2012. Teaching hydrological modeling with a user-friendly catchment-runoff-model software package. Hydrol. Earth Syst. Sci. 16 (9), 3315–3325. https://doi.org/10.5194/hess-16-3315-2012.
Seibert, J., Bergström, S., 2022. A retrospective on hydrological catchment modelling based on half a century with the HBV model. Hydrol. Earth Syst. Sci. 26 (5), 1371–1388. https://doi.org/10.5194/hess-26-1371-2022.
Shin, M.-J., Guillaume, J.H.A., Croke, B.F.W., Jakeman, 2013. Addressing ten questions about conceptual rainfall–runoff models with global sensitivity analyses in R. Journal of Hydrology 503, 135–152. https://doi.org/10.1016/j.jhydrol.2013.08.047.
Shuttleworth, W.J., Wallace, J.S., 1985. Evaporation from sparse crops: an energy combination theory. Q. J. R. Meteorolog. Soc. 111, 839–855.
Smirnova, E., Bergeron, Y., Brais, S., Granström, A., 2008. Postfire root distribution of Scots pine in relation to fire behaviour. Can. J. For. Res. 38, 353–362. https://doi.org/10.1139/X07-127.
Sobol, I.M., 2001. Global sensitivity indices for nonlinear mathematical models and their Monte Carlo estimates. Math. Comput. Simul 55, 271–280. https://doi.org/10.1016/S0378-4754(00)00270-6.
Song, X., Zhang, J., Zhan, C., Xuan, Y., Ye, M., Xu, C., 2015. Global sensitivity analysis in hydrological modeling: review of concepts, methods, theoretical framework, and applications. J. Hydrol. 523, 739–757. https://doi.org/10.1016/j.jhydrol.2015.02.013.
Song, X., Gao, X., Dyck, M., Zhang, W., Wu, P., Yao, J., Zhao, X., 2018. Soil water and root distribution of apple tree (Malus pumila Mill) stands in relation to stand age and rainwater collection and infiltration system (RWCI) in a hilly region of the Loess Plateau, China. Catena 170, 324–334. https://doi.org/10.1016/j.catena.2018.06.026.
Taconet, O., Bernard, R., Vidal-Madjar, D., 1986. Evapotranspiration over an agricultural region using a surface flux/temperature model based on NOAA-AVHRR data. J. Clim. Appl. Meteorol. 25, 284–307. https://doi.org/10.1175/1520-0450(1986)025<0284:EOAARU>2.0.CO;2.
Tafasca, S., Ducharne, A., Valentin, C., 2020. Weak sensitivity of the terrestrial water budget to global soil texture maps in the ORCHIDEE land surface model. Hydrol. Earth Syst. Sci. 24, 3753–3774. https://doi.org/10.5194/hess-24-3753-2020.
Tardieu, F., Katerji, N., Bethenod, O., Zhang, J., Davies, W.J., 1991. Maize stomatal conductance in the field: its relationship with soil and plant water potentials, mechanical constraints and ABA concentration in the xylem sap. Plant Cell Environ. 14, 121–126. https://doi.org/10.1111/j.1365-3040.1991.tb01378.x.
van Dam, J.C., Groenendijk, P., Hendriks, R.F.A., Kroes, J.G., 2008. Advances of modeling water flow in variably saturated soils with SWAP. Vadose Zone J. 7, 640–653. https://doi.org/10.2136/vzj2007.0060.
Van Wijk, W., Scholte Ubing, D., 1963. Radiation. In: Van Wijk, W. (Ed.), Physics of Plant Environment. North-Holland Publishing Company, pp. 62–101.
Vemuri, V., Dracup, J.A., Erdmann, R.C., Vemuri, N., 1969. Sensitivity analysis method of system identification and its potential in hydrologic research. Water Resour. Res. 5 (2), 341–349. https://doi.org/10.1029/WR005i002p00341.
Vidal, J.-P., Martin, E., Franchistéguy, L., Baillon, M., Soubeyroux, J.-M., 2010. A 50-year high-resolution atmospheric reanalysis over France with the Safran system. Int. J. Climatol. 30, 1627–1644. https://doi.org/10.1002/joc.2003.
Wiltshire, A.J., Rojas, C.D., Edwards, J., Gedney, N., Harper, A.B., Hartley, A., Hendry, M.A., Robertson, E., Smout-Day, K., 2019. JULES-GL7: The global land configuration of the Joint UK Land Environment Simulation version 7.0. Geoscientific Model Development Discussions. doi: 10.5194/gmd-2019-152.

Wang, Z.-M., Batelaan, O., De Smedt, F., 1996. A distributed model for water and energy transfer between soils, plants and atmosphere (WetSpa). Physics and Chemistry of the Earth 21 (3), 189–193.

Wang, J., Li, X., Lu, L., Fang, F., 2013. Parameter sensitivity analysis of crop growth models based on the extended Fourier Amplitude Sensitivity Test method. Environmental modelling & software 48, 171–182.

Winkel, T., Rambal, S., 1993. Influence of water stress on grapevines growing in the field: from leaf to whole-plant response. Funct. Plant Biol. 20, 143. https://doi.org/10.1071/PP9930143.

Yang, J., Liu, Y., Yang, W., Chen, Y., 2012. Multi-Objective sensitivity analysis of a fully distributed hydrologic model wetspa. Water Resour. Manag. 26 (1), 109–128.

Yokohata, T., Kinoshita, T., Sakurai, G., Pokhrel, Y., Ito, A., Okada, M., Satoh, Y., Kato, E., Nitta, T., Fujimori, S., Felfelani, F., Masaki, Y., Iizumi, T., Nishimori, M., Hanasaki, N., Takahashi, K., Yamagata, Y., Emori, S., 2019. MIROC-INTEG1: a global bio-geochemical land surface model with human water management, crop growth, and land-use change. Geosci. Model Dev. Discuss. https://doi.org/10.5194/gmd-2019-184.

Zeighami, F., Sandoval, L., Guadagnini, A., Di Federico, V., 2023. Uncertainty quantification and global sensitivity analysis of seismic metabarriers. Eng. Struct. 277, 115415. https://doi.org/10.1016/j.engstruct.2022.115415.

Zhang, L., Hu, Z., Fan, J., Zhou, D., Tang, F., 2014. A meta-analysis of the canopy light extinction coefficient in terrestrial ecosystems. Front. Earth Sci. 8, 599–609. https://doi.org/10.1007/s11707-014-0446-7.

Zhang, Y., Oren, R., Kang, S., 2012. Spatiotemporal variation of crown-scale stomatal conductance in an arid Vitis vinifera L. cv. Merlot vineyard: Direct effects of hydraulic properties and indirect effects of canopy leaf area. Tree Physiol. 32, 262–279. https://doi.org/10.1093/treephys/tpr120.